J Elast
https://doi.org/10.1007/s10659-020-09772-x

Indentation of a Periodically Layered, Planar, Elastic Half-Space

Deepak Sachan[1] · Ishan Sharma[1] · T. Muthukumar[2]

Received: 12 November 2019

Abstract We investigate indentation by a smooth, rigid indenter of a two-dimensional half-space comprised of periodically arranged linear-elastic layers with different constitutive responses. Identifying the half-space's material parameters as periodic functions in space, we utilize the theory of periodic homogenization to approximate the layered *heterogeneous* material by a linear-elastic, *homogeneous*, but *anisotropic* medium. This approximation becomes exact as the layer thickness becomes infinitesimal. In this way, we reduce the original problem to the indentation of an anisotropic, homogeneous, linear-elastic half-space by a smooth, rigid indenter. The latter is solved analytically by formulating and resolving the corresponding matrix Riemann–Hilbert boundary-value problem in complex analysis. Thus, we obtain an approximate, but analytical solution for the indentation of a layered heterogeneous medium. We then compare this solution with finite element computations of the indentation on the original layered, heterogenous half-space. We conclude that (a) the contact pressure on the layered, heterogenous half-space is well approximated by that obtained through homogenization, and the approximation improves as the layer thickness is decreased, or if the indentation force is increased; (b) the upper bound of the difference between the two contact pressures depends only upon the ratio of the Young's moduli of the two materials constituting the heterogenous medium and their Poisson's ratio; and (c) the average variation of the discontinuous von Mises stress in the layered half-space is well approximated by the one found in the homogenized half-space. The approach presented here can be utilized for a diverse array of indentation and contact problems of finely mixed heterogeneous media, and is also amenable to systematic improvements.

✉ D. Sachan
dsachan@iitk.ac.in

I. Sharma
ishans@iitk.ac.in

T. Muthukumar
tmk@iitk.ac.in

[1] Mechanics & Applied Mathematics Group, Department of Mechanical Engineering, Indian Institute of Technology Kanpur, Kanpur, 208016, India

[2] Mechanics & Applied Mathematics Group, Department of Mathematics & Statistics, Indian Institute of Technology Kanpur, Kanpur, 208016, India

Published online: 07 May 2020

Keywords Indentation · Heterogeneous media · Layered media · Homogenization · Anisotropy · Elasticity

Mathematics Subject Classification (2010) 74B05 · 74E05 · 74E10 · 74G05 · 74G15 · 74M15 · 74Q05 · 74S05

1 Introduction

Indentation in elastic materials is a classical and important engineering problem. Commonly occurring phenomena such as rail wheels on a railroad, penetration of a syringe in a body tissue, are examples of indentation processes. Mechanical properties of materials are routinely measured using instrumented indentation machines [1, 2]. Indentation is also prevalent in various manufacturing processes, such as in forming.

Closed-form solutions for primary variables of interest, such as the pressure in the contact region or the stress field in the indented material are known for the indentation of an isotropic elastic half-space [3, 4]. Green and Zerna [5] investigated the plane-strain indentation of an anisotropic elastic half-space and provided analytical expressions of the stress field, but follow a rather involved process. Fan and Keer [6] reconsidered the work of [5] and simplified it utilizing the compact formalism of Stroh [7]; however they did not solve the indentation problem. More importantly, all such investigations have been carried out only for homogeneous elastic media. At the same time, the importance of heterogeneous media is well-known in engineering applications: composites, soil, and tissue, for example, are all heterogeneous. Hence, there is a need to investigate indentation into heterogeneous elastic materials.

Phrasing linear-elastic problems in the displacement formulation involves second-order linear elliptic partial differential equations (PDEs), which can be solved exactly for very few systems with simple constitutive description, loading conditions and geometry. In these PDEs, and in the boundary data relevant to the system for a heterogeneous medium, the material coefficients vary with space, which further complicates the problem.

Here, we study indentation of a layered medium, one of the simplest examples of heterogeneous media. Layered media abound in nature and industrial applications. Many such instances of layered media and the typical loads that they carry can be considered as constituting problems of indentation, for example, ceramics used in space shuttles, and the load acting on them during atmospheric re-entry, vehicle tyre on a road, bone interacting with articular cartilage and woodpecker pecking a tree made of different layers of wood etc. Mammalian skin, cell wall, artery wall are all layered media and indentation is often used to find their elastic properties.

In this work, we investigate indentation of a half-space consisting of layers of two isotropic elastic materials stacked periodically atop each other. Analytical investigation of this problem is hard. However progress may be achieved if we consider layers of infinitesimal thickness. In this limit, we use the results of the theory of periodic homogenization to show that the elastic behavior of this layered medium, when homogenized, is exactly the same as that of an *anisotropic, homogeneous* elastic material, the indentation problem on which may be solved exactly. The main utility of such an analysis lies in the investigation of layered media with layers of small thickness. At the same time, the numerical investigation of such finely-layered media is made difficult by the rapid fluctuations in the material coefficients. However, as is shown in this work, the relevant physical quantities can be very well approximated by those of the limiting 'homogenized' material.

Homogenization is known to work best in the bulk. However, in indentation problems we are primarily interested in surface quantities, such as the pressure profile under the indenter. Thus, we also carry out the numerical simulation of indentation of finely-layered media to investigate the convergence of pressure under the indenter to that of the homogenized material, while changing several relevant physical parameters controlling the problem: the force on the indenter, radius of the indenter, Young's moduli of the materials constituting the layered medium, and the thickness of its layers.

The outline of the article is as follows. In Sect. 2, the contact problem of a general medium is formulated, which is then specialized to a planar indentation boundary value problem. In Sect. 3, we consider the plane strain indentation problem of a homogeneous, anisotropic half-space and find the closed-form expressions for contact pressure and the stress fields within the indented material. We then consider the indentation on a layered medium in Sect. 4. Assuming a finely-layered medium, we proceed by homogenizing the medium. We find the closed-form expressions for the components of the stiffness tensor of the homogenized material and observe that the homogenized material is anisotropic, specifically *transversely isotropic*. We the utilize results from Sect. 3 to obtain contact pressure and stress fields in closed-form on the homogenized material for a layered half-space comprising layers of two isotropic, homogeneous materials of equal thickness in an infinite periodic arrangement. Finally, in Sect. 5, results for indentation of layered media, obtained through a finite element (FE) analysis, are discussed and compared with our analytical results. It is shown, by defining an appropriate error variable, that the pressure profile under the indenter in the layered medium converges to that of the homogenized material as the layer thickness in the layered medium is decreased, or if the force on the indenter is increased. It is also shown that the upper bound of this error variable depends only upon the ratio of the Young's moduli of the two constituent materials and their Poisson's ratio. We also investigate the maximum of the von Mises stress in the layered media, which is important from the point of view of applications. This is then followed by conclusions in Sect. 6.

We will be presenting subsequent development beginning with a three-dimensional setting, even though we will quickly specialize to a two-dimensional problem. Similarly, the reader may find some well-known results/facts laid out in some detail. Our reasons for doing so are two-fold: (a) to prepare grounds for seamless extension to three-dimensional problems, and (b) to clearly identify typical assumptions which will be important whenever we seek to improve the errors inherent in applying homogenization techniques near boundaries.

2 Indentation Problem: General Formulation for a Smooth Indenter

We begin by considering the indentation of a three-dimensional, linear-elastic, heterogeneous body, occupying the half-space $\Omega := \mathbb{R} \times (0, \infty) \times \mathbb{R}$ by a rigid, smooth, circular cylindrical indenter with radius R. Figures 1a and b illustrate the body after and before indentation, respectively. Both Figs. 1a and b are cross-sections of the system in the x_1-x_2 plane. Let O denote the origin in Fig. 1b. We assume that the line force F pressing upon the indenter passes through the indenter's central axis and the direction of F is along the x_2-axis. Given this loading condition, the indenter contacts the body over a contact region $\Gamma_1 := (-L, L) \times \{0\} \times \mathbb{R}$, for some length $L > 0$ of the contact region. We assume that a priori, either the *contact length* $2L$ or the loading F is known. We take the body forces to be zero and the strains to be small. We shall impose a mixed boundary condition on Γ_1 in terms of the stress and the partial derivatives of the vertical displacement along the x_2-axis. The stress condition on Γ_1 is obtained from a consideration of zero friction under the smooth

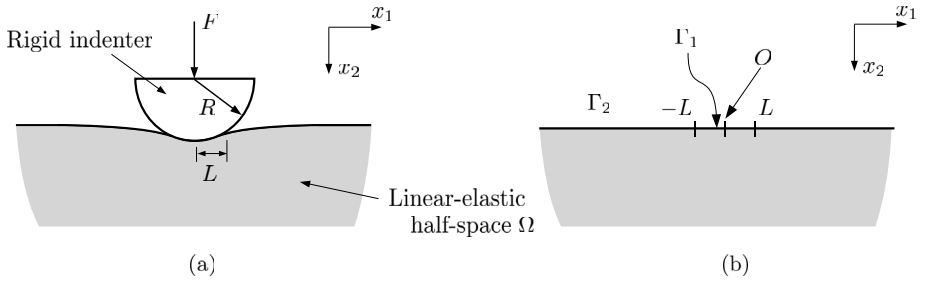

Fig. 1 Indentation on a three-dimensional half-space Ω viewed along the x_3-axis. (**a**) Sketch of the physical problem. (**b**) The mathematical model assuming that the material is linear-elastic and the strains are small, so that the boundary conditions are applied upon the *un*deformed boundary.

indenter, because of which the traction components along the x_1- and x_3-axes are zero. The displacement condition on Γ_1 results by virtue of the indenter being rigid, so that the material on Γ_1 takes the shape of indenter. Thus, if $\mathbf{v}(x_1, x_3) = (v_1(x_1, x_3), v_2(x_1, x_3), v_3(x_1, x_3))$ denotes the displacement of Γ_1, $\partial v_2/\partial x_1$ and $\partial v_2/\partial x_3$ are then known on Γ_1. Because $\Gamma_2 := \partial\Omega \setminus \Gamma_1$[1] is a free boundary, we impose zero traction on Γ_2 in all three directions. The mathematical formulation of indentation is hence provided by the following boundary value problem in displacement formulation, using Einstein's summation convention:

$$\begin{cases} \dfrac{\partial}{\partial x_j}\left(a_{ijkh}\dfrac{\partial u_k}{\partial x_h}\right) = 0 \quad \text{in } \Omega, \quad i = 1, 2, 3, \\ \dfrac{\partial \mathbf{u}}{\partial x_i} \cdot \mathbf{e_2} = \dfrac{\partial v_2}{\partial x_i}, \quad a_{ijkh}\dfrac{\partial u_k}{\partial x_h} n_j = 0 \quad \text{on } \Gamma_1, \quad i = 1, 3, \\ a_{ijkh}\dfrac{\partial u_k}{\partial x_h} n_j = 0 \quad \text{on } \Gamma_2, \quad i = 1, 2, 3, \end{cases} \tag{1}$$

where $\mathbf{u}(\mathbf{x}) = (u_1(\mathbf{x}), u_2(\mathbf{x}), u_3(\mathbf{x}))$ is the unknown three-dimensional *displacement*, $\partial v_2/\partial x_1$ and $\partial v_2/\partial x_3$ are known on Γ_1, $a_{ijkh}(\mathbf{x})$ are the components of a fourth-order *stiffness tensor* that characterizes the material's linear-elastic response and may vary spatially, the boundary of Ω is $\partial\Omega = \Gamma_1 \bigcup \Gamma_2 = \mathbb{R} \times \{0\} \times \mathbb{R}$, and $\mathbf{n}(\mathbf{x}) = (n_1(\mathbf{x}), n_2(\mathbf{x}), n_3(\mathbf{x}))$ is the unit outward normal on the boundary $\partial\Omega$. The components $\epsilon_{ij}(\mathbf{x}) = \epsilon_{ji}(\mathbf{x})$ of the *strain tensor* $\underline{\underline{\epsilon}}$ are found from the displacement field $\mathbf{u}$ by

$$\epsilon_{ij}(\mathbf{x}) = \frac{1}{2}\left(\frac{\partial u_i}{\partial x_j} + \frac{\partial u_j}{\partial x_i}\right), \tag{2}$$

while the components $\sigma_{ij}(\mathbf{x}) = \sigma_{ji}(\mathbf{x})$ of the *stress tensor* are related to those of the strain tensor by the generalized Hooke's law:

$$\sigma_{ij}(\mathbf{x}) = a_{ijkh}(\mathbf{x})\,\epsilon_{kh}(\mathbf{x}). \tag{3}$$

The stiffness tensor is assumed positive-definite and satisfies

$$a_{ijkh}(\mathbf{x}) = a_{jikh}(\mathbf{x}) = a_{ijhk}(\mathbf{x}) = a_{khij}(\mathbf{x}). \tag{4}$$

[1] Given two sets A and B, the set $A \setminus B := \{x \in A \mid x \notin B\}$ is the relative complement of B in A.

We wish to compute the pressure under the indenter, i.e. on Γ_1, and the von Mises stress in Ω. Pressure on Γ_1 is given by $p(x_1, x_3) := -\sigma_{22}(x_1, 0, x_3)$. The von Mises stress, denoted by σ_{VM}, is a scalar defined by

$$\sigma_{\text{VM}}(\mathbf{x}) := \frac{1}{\sqrt{2}}\sqrt{(\sigma_{11}-\sigma_{22})^2 + (\sigma_{22}-\sigma_{33})^2 + (\sigma_{33}-\sigma_{11})^2 + 6(\sigma_{12}^2 + \sigma_{23}^2 + \sigma_{13}^2)}. \tag{5}$$

The maximum value of σ_{VM} is often utilized to predict the onset of plastic behavior in ductile materials [8]. It has not been possible to solve the indentation problem (1) for a general choice of a_{ijkh} to obtain closed-form expressions of $p(x_1, x_3)$ and $\sigma_{\text{VM}}(\mathbf{x})$. To make progress, we now make the following two assumptions on (1):
(H1) Material undergoes *plane strain* deformation, which assumes that the displacement field $\mathbf{u}(\mathbf{x})$ satisfies:

$$u_1(\mathbf{x}) = u_1(x_1, x_2), u_2(\mathbf{x}) = u_2(x_1, x_2) \text{ and } u_3(\mathbf{x}) = 0, \tag{6}$$

which, using (2), implies $\epsilon_{ij}(\mathbf{x}) = \epsilon_{ij}(x_1, x_2)$ for $i, j = 1, 2$, and $\epsilon_{k3}(\mathbf{x}) = 0$ for $k = 1, 2, 3$. The displacement of Γ_1 also simplifies as $\mathbf{v}(x_1, x_3) = \mathbf{v}(x_1) = (v_1(x_1), v_2(x_1), 0)$.
(H2) To admit plane strain the elastic coefficients a_{ijkh} of the material must satisfy

$$\begin{aligned} &a_{1113} = a_{1123} = a_{2213} = a_{2223} = a_{1213} = a_{1223} = 0, \\ \text{and} \qquad &a_{ij33}(\mathbf{x}) = a_{ij33}(x_1, x_2), \quad i, j = 1, 2. \end{aligned} \tag{7}$$

The assumption (7) is not too restrictive, because many physical materials, including monoclinic materials with the symmetry plane at $x_3 = 0$ satisfy it in general. In particular, the layered media, which we study in Sect. 4, also satisfy (7).

Employing (2) and (3), along with assumptions (6) and (7), we obtain $\sigma_{ij}(\mathbf{x}) = \sigma_{ij}(x_1, x_2)$ for $i, j = 1, 2$ and $\sigma_{k3}(\mathbf{x}) = 0$ for $k = 1, 2$ and also $p(x_1, x_3) = p(x_1)$. Thus, from (5), we obtain

$$\sigma_{\text{VM}}(\mathbf{x}) = \sigma_{\text{VM}}(x_1, x_2) = \frac{1}{\sqrt{2}}\sqrt{(\sigma_{11}-\sigma_{22})^2 + (\sigma_{22}-\sigma_{33})^2 + (\sigma_{33}-\sigma_{11})^2 + 6\sigma_{12}^2}. \tag{8}$$

With (6) and (7), (1) turns into the following, essentially *two*-dimensional problem:

$$\begin{cases} \dfrac{\partial}{\partial x_j}\left(a_{ijkh}\dfrac{\partial u_k}{\partial x_h}\right) = 0 \quad \text{in } \Omega, \quad i = 1, 2, & \text{(9a)} \\ \dfrac{\partial \mathbf{u}}{\partial x_1} \cdot \mathbf{e_2} = \dfrac{dv_2}{dx_1} \quad \text{on } \Gamma_1, & \text{(9b)} \\ a_{1jkh}\dfrac{\partial u_k}{\partial x_h} n_j = 0 \quad \text{on } \Gamma_1, & \text{(9c)} \\ a_{ijkh}\dfrac{\partial u_k}{\partial x_h} n_j = 0 \quad \text{on } \Gamma_2, \quad i = 1, 2. & \text{(9d)} \end{cases}$$

For a homogeneous, isotropic half-space Ω, Muskhelishvili [3] provides a general method to find the components of the stress tensor $\sigma_{ij}(x_1, x_2)$, in particular $p(x_1)$, for an

arbitrarily shaped indenter. For future use, we quickly recall the result for a parabolic indenter with the profile $x_2 = -x_1^2/(2R)$. For a homogeneous, isotropic material, a_{ijkh}'s are constant functions given by

$$a_{ijkh} = \lambda\, \delta_{ij}\delta_{kh} + \mu\, (\delta_{ih}\delta_{jk} + \delta_{ik}\delta_{jh}), \tag{10}$$

where $\lambda \geq 0$ and $\mu > 0$ are *Lamé's* parameters and δ_{ij} is the Kronecker delta symbol. Clearly, (10) satisfies the assumptions (7). Then for a homogeneous, isotropic half-space Ω, the pressure profile is provided by

$$p(x_1) = \frac{1}{R}\frac{4\mu}{\chi+1}\sqrt{L^2 - x_1^2} = \frac{1}{R}\frac{E}{2(1-\nu^2)}\sqrt{L^2 - x_1^2} \quad \text{on } \Gamma_1, \tag{11}$$

where the Young's modulus E and Poisson's ratio ν of the isotropic material are

$$E = \frac{\mu(3\lambda + 2\mu)}{\lambda + \mu}, \quad \nu = \frac{\lambda}{2(\lambda+\mu)} \quad \text{and} \quad \chi = \frac{\lambda + 3\mu}{\lambda + \mu}. \tag{12}$$

A circular indenter with radius R can be approximated by a parabolic indenter on Γ_1, i.e. on $-L < x_1 < L$ if we assume that $R \gg L$, as we will do. Stress components are found using a complex-valued function $h : \mathbb{C} \setminus \{z \in \mathbb{C} \mid x_2 > 0\} \to \mathbb{C}$ as

$$\sigma_{22}(x_1, x_2) - i\,\sigma_{21}(x_1, x_2) = h(z) - h(\bar{z}) + (z - \bar{z})\overline{\frac{dh}{dz}(z)},$$

and

$$\sigma_{11}(x_1, x_2) + \sigma_{22}(x_1, x_2) = 2[h(z) + \overline{h(z)}], \tag{13}$$

where

$$h(z) = \frac{2\mu i z}{R(\chi+1)} + \frac{2\mu}{R(\chi+1)}\sqrt{L^2 - z^2}, \tag{14}$$

$z = x_1 + i x_2$ is a complex variable and the overbar '¯' indicates the complex conjugate. We find $\sigma_{33}(x_1, x_2)$ by substituting (4) in (3) and utilizing (6), (10) and (12) to obtain

$$\sigma_{33} = \nu(\sigma_{11} + \sigma_{22}). \tag{15}$$

Subsequently, we may compute σ_{VM} from (8).

In this article, we are interested in the plane strain indentation of a heterogeneous, linear-elastic, half-space Ω. For a heterogeneous medium a_{ijkh} vary spatially. In general, even in the planar case, for heterogeneous media, there exist no closed-form expressions for $p(x_1)$ and $\sigma_{\text{VM}}(\mathbf{x})$. Therefore, as a first step, we consider the case of planar, layered media. For a finely-layered medium, we will utilize homogenization techniques in Sect. 4 to convert the heterogeneous, layered medium into a homogeneous, but *anisotropic*, material. Once that is done, we will have to investigate the plane strain indentation of a homogeneous, anisotropic material, which we do so next.

3 Plane Strain Indentation of a Homogeneous, Anisotropic Half-Space

We now investigate plane strain indentation of a homogeneous, anisotropic half-space satisfying (7). For a homogeneous, anisotropic material a_{ijkh}'s are constant functions, but two

parameters such as λ and μ, are no longer sufficient, complicating the analysis of the indentation problem. Fan and Keer [6] investigate the plane-strain indentation of a homogeneous, anisotropic half-space utilizing the compact formalism of Stroh [7], and then employing an analytic function continuation approach to arrive at a matrix Riemann–Hilbert (RH) problem. However, they do not motivate their ansatz for the displacement field that they assume. Moreover, they stop short of actually solving the RH problem, so that the indentation problem remains unsolved. In this section, we follow the formulation of [6], but present better motivated and more transparent approach by starting with the equilibrium equations (9a). We eventually arrive at the corresponding matrix RH problem, which is then solved to obtain the closed-form expressions for the contact pressure $p(x_1)$, stress field $\underline{\underline{\sigma}}(\mathbf{x})$ and the von Mises stress $\sigma_{\mathrm{VM}}(\mathbf{x})$ inside the anisotropic half-space.

Under plane strain conditions (6), (9a) may be written in terms of the stress components as

$$\frac{\partial \sigma_{11}}{\partial x_1} + \frac{\partial \sigma_{12}}{\partial x_2} = 0 \quad \text{and} \quad \frac{\partial \sigma_{21}}{\partial x_1} + \frac{\partial \sigma_{22}}{\partial x_2} = 0 \quad \text{in } \Omega. \tag{16}$$

We introduce scalar fields $\phi_1(x_1, x_2)$ and $\phi_2(x_1, x_2)$ such that

$$\sigma_{i1} = -\frac{\partial \phi_i}{\partial x_2} \quad \text{and} \quad \sigma_{i2} = \frac{\partial \phi_i}{\partial x_1} \quad \text{for } i = 1, 2, \tag{17}$$

so that (16) are automatically satisfied. Invoking (2) and (3) to replace the stress components, we write (17) in terms of the displacement as

$$\mathbf{Q}\begin{pmatrix} \dfrac{\partial u_1}{\partial x_1} \\ \dfrac{\partial u_2}{\partial x_1} \end{pmatrix} + \mathbf{R}\begin{pmatrix} \dfrac{\partial u_1}{\partial x_2} \\ \dfrac{\partial u_2}{\partial x_2} \end{pmatrix} = -\begin{pmatrix} \dfrac{\partial \phi_1}{\partial x_2} \\ \dfrac{\partial \phi_2}{\partial x_2} \end{pmatrix} \quad \text{and} \quad \mathbf{R}^T\begin{pmatrix} \dfrac{\partial u_1}{\partial x_1} \\ \dfrac{\partial u_2}{\partial x_1} \end{pmatrix} + \mathbf{W}\begin{pmatrix} \dfrac{\partial u_1}{\partial x_2} \\ \dfrac{\partial u_2}{\partial x_2} \end{pmatrix} = \begin{pmatrix} \dfrac{\partial \phi_1}{\partial x_1} \\ \dfrac{\partial \phi_2}{\partial x_1} \end{pmatrix}, \tag{18}$$

where

$$\mathbf{Q} := (a_{i1k1}), \quad \mathbf{R} := (a_{i1k2}) \quad \text{and} \quad \mathbf{W} := (a_{i2k2}) \tag{19}$$

are 2×2 matrices and the superscript 'T' denotes the transpose of a matrix. Note that $\mathbf{Q}$ and $\mathbf{W}$ are symmetric matrices. We introduce

$$\mathbf{S_1} := \begin{bmatrix} -\mathbf{R}^T & \mathbf{I} \\ -\mathbf{Q} & \mathbf{0} \end{bmatrix}, \quad \mathbf{S_2} := \begin{bmatrix} \mathbf{W} & \mathbf{0} \\ \mathbf{R} & \mathbf{I} \end{bmatrix} \quad \text{and} \quad \mathbf{Y} := \begin{pmatrix} u_1 \\ u_2 \\ \phi_1 \\ \phi_2 \end{pmatrix}, \tag{20}$$

where $\mathbf{I}$ and $\mathbf{0}$ are the 2×2 identity and zero matrices, respectively, and rewrite (18) in the form of a coupled system of first-order partial differential equations as

$$\mathbf{S_1}\frac{\partial \mathbf{Y}}{\partial x_1} = \mathbf{S_2}\frac{\partial \mathbf{Y}}{\partial x_2}. \tag{21}$$

Utilizing the positive-definiteness of the stiffness tensor, we find that $\mathbf{Q}$ and $\mathbf{W}$ are also positive-definite, hence nonsingular. Therefore, both $\mathbf{S_1}^{-1}$ and $\mathbf{S_2}^{-1}$ exist, and (21) may be

written as

$$\mathbf{S_2}^{-1}\mathbf{S_1}\frac{\partial \mathbf{Y}}{\partial x_1} = \frac{\partial \mathbf{Y}}{\partial x_2}. \tag{22}$$

We now wish to diagonalize $\mathbf{S_2}^{-1}\mathbf{S_1}$ over the field of complex numbers $\mathbb{C}$ and set

$$\mathbf{S_2}^{-1}\mathbf{S_1} = \mathbf{E}\boldsymbol{\Lambda}\mathbf{E}^{-1}, \tag{23}$$

where $\boldsymbol{\Lambda} = \mathrm{diag}(\Lambda_1, \Lambda_2, \bar{\Lambda}_1, \bar{\Lambda}_2)$ is the diagonal matrix formed by the four eigenvalues and the matrix $\mathbf{E}$ is obtained by having the eigenvectors corresponding to the four eigenvalues as its column vectors. Because $\mathbf{S_1}$ and $\mathbf{S_2}$ depend only upon material coefficients a_{ijkh}, which are constant functions, therefore $\mathbf{E}$ and $\boldsymbol{\Lambda}$ also are constant functions. Thus, we may rewrite (22) as

$$\boldsymbol{\Lambda}\frac{\partial(\mathbf{E}^{-1}\mathbf{Y})}{\partial x_1} = \frac{\partial(\mathbf{E}^{-1}\mathbf{Y})}{\partial x_2},$$

which is a system of constant coefficient linear first-order PDEs. This equation has solutions of the form

$$\mathbf{Y} = \begin{pmatrix} u_1 \\ u_2 \\ \phi_1 \\ \phi_2 \end{pmatrix} = \mathbf{E}\begin{pmatrix} f_1(z_1) \\ f_2(z_2) \\ f_3(\bar{z}_1) \\ f_4(\bar{z}_2) \end{pmatrix}, \tag{24}$$

where $f_i(x_1 + \Lambda_i x_2)$, for $i = 1, 2$, are holomorphic functions of the complex variables $z_i := x_1 + \Lambda_i x_2$ and $f_{i+2}(x_1 + \bar{\Lambda}_i x_2)$, for $i = 1, 2$, are holomorphic functions of the variable $\bar{z}_i = x_1 + \bar{\Lambda}_i x_2$; here $x_1 \in \mathbb{R}$ and $x_2 > 0$. We rewrite $\mathbf{E}$ in the block matrix notation, using two 2×2 matrices $\mathbf{A}$ and $\mathbf{B}$, as

$$\mathbf{E} = \begin{bmatrix} \mathbf{A} & \bar{\mathbf{A}} \\ \mathbf{B} & \bar{\mathbf{B}} \end{bmatrix}, \tag{25}$$

which follows from the fact that the eigenvectors making up $\mathbf{E}$'s columns are complex conjugates. Clearly, if $\mathbf{A} = (A_{ij})$ and $\mathbf{B} = (B_{ij})$ then, utilizing (19) and the diagonalization of $\mathbf{S_2}^{-1}\mathbf{S_1}$, we must have [9]

$$B_{ij} = \sum_{k=1}^{2}(a_{i2k1} + \Lambda_j a_{i2k2})A_{kj}. \tag{26}$$

Because $\mathbf{u}(x_1, x_2)$ is real, we further obtain from (24) and (25) that $f_{i+2}(\bar{z}_i) = \overline{f_i(z_i)}$ for $i = 1, 2$, which then provides the following general solution:

$$\mathbf{u}(x_1, x_2) = 2\mathrm{Re}\left\{\mathbf{A}\begin{pmatrix} f_1(z_1) \\ f_2(z_2) \end{pmatrix}\right\} \quad \text{and} \quad \begin{pmatrix} \phi_1 \\ \phi_2 \end{pmatrix}(x_1, x_2) = 2\mathrm{Re}\left\{\mathbf{B}\begin{pmatrix} f_1(z_1) \\ f_2(z_2) \end{pmatrix}\right\}, \tag{27}$$

where $\mathrm{Re}\{\cdot\}$ denotes the real part of the complex expression inside the braces. Utilizing (17) and (27) provides the following expressions of the stress fields:

$$\sigma_{i2}(x_1,x_2)=2\mathrm{Re}\left\{\mathbf{B}\begin{pmatrix}\dfrac{df_1}{dz_1}(z_1)\\[2ex]\dfrac{df_2}{dz_2}(z_2)\end{pmatrix}\right\}\quad\text{and}\quad\sigma_{i1}(x_1,x_2)=-2\mathrm{Re}\left\{\mathbf{B}\begin{pmatrix}\Lambda_1\dfrac{df_1}{dz_1}(z_1)\\[2ex]\Lambda_2\dfrac{df_2}{dz_2}(z_2)\end{pmatrix}\right\}. \tag{28}$$

Now employing (27), the displacement in the contact region Γ_1 may be written as

$$\mathbf{A}\begin{pmatrix}f_1(x_1)\\f_2(x_1)\end{pmatrix}+\bar{\mathbf{A}}\begin{pmatrix}\overline{f_1(x_1)}\\\overline{f_2(x_1)}\end{pmatrix}=\begin{pmatrix}v_1(x_1)\\v_2(x_1)\end{pmatrix},\quad x_1\in\Gamma_1. \tag{29}$$

Similarly, invoking (9c) and (28), the surface traction on Γ_1 is found to be

$$\mathbf{B}\begin{pmatrix}\dfrac{df_1}{dz_1}(z_1)\\[2ex]\dfrac{df_2}{dz_2}(z_2)\end{pmatrix}\Bigg|_{x_2=0}+\bar{\mathbf{B}}\begin{pmatrix}\overline{\dfrac{df_1}{dz_1}(z_1)}\\[2ex]\overline{\dfrac{df_2}{dz_2}(z_2)}\end{pmatrix}\Bigg|_{x_2=0}=\begin{pmatrix}0\\\sigma_{22}(x_1,0)\end{pmatrix},\quad x_1\in\Gamma_1. \tag{30}$$

We now introduce a function $\mathbf{h}:\mathbb{C}\setminus\{z\in\mathbb{C}\mid x_2=0\}\to\mathbb{C}^{2\times1}$ as follows:

$$\mathbf{h}(z)=\begin{pmatrix}h_1(z)\\h_2(z)\end{pmatrix}:=\begin{cases}\mathbf{B}\begin{pmatrix}\dfrac{df_1}{dz_1}(z)\\[2ex]\dfrac{df_2}{dz_2}(z)\end{pmatrix}, & z\in S^+:=\{z\in\mathbb{C}\mid x_2>0\},\\[4ex]-\bar{\mathbf{B}}\begin{pmatrix}\overline{\dfrac{df_1}{dz_1}(\bar z)}\\[2ex]\overline{\dfrac{df_2}{dz_2}(\bar z)}\end{pmatrix}, & z\in S^-:=\{z\in\mathbb{C}\mid x_2<0\},\end{cases} \tag{31}$$

where $z=x_1+ix_2$ is the complex variable locating a point in the elastic half-space's interior. Clearly, $\mathbf{h}$ is a holomorphic function. Using the traction free condition (9d) on Γ_2, along with (28) and (31), we observe that $\mathbf{h}^+(x_1)=\mathbf{h}^-(x_1)$ on Γ_2, where $\mathbf{h}^+(x_1)=\lim\limits_{\substack{z\to x_1\in\Gamma_1\bigcup\Gamma_2,\\ z\in S^+}}\mathbf{h}(z)$ and $\mathbf{h}^-(x_1)=\lim\limits_{\substack{z\to x_1\in\Gamma_1\bigcup\Gamma_2,\\ z\in S^-}}\mathbf{h}(z)$. Therefore, the values of $\mathbf{h}(z)$ in S^+ and S^- can be considered as the analytic continuation of one another through Γ_2. Hence, we regard $\mathbf{h}(z)$ as a holomorphic function in $\mathbb{C}\setminus\Gamma_1$. Such a function is called a *sectionally analytic* function. Introducing

$$\mathbf{t}(x_1)=\begin{pmatrix}0\\t_2(x_1)\end{pmatrix}:=\begin{pmatrix}0\\\sigma_{22}(x_1,0)\end{pmatrix}, \tag{32}$$

we write (30) as

$$\mathbf{h}^+(x_1)-\mathbf{h}^-(x_1)=\mathbf{t}(x_1),\quad x_1\in\Gamma_1. \tag{33}$$

We wish to find a sectionally analytic function $\mathbf{h}(z)$ which satisfies (33). Such a problem is called a *Riemann–Hilbert (RH) problem* (see [3, 10]). Utilising the Sokhotski–Plemelj formula [3, 10] in (33), we immediately obtain

$$\mathbf{h}^{\pm}(x_1) = \frac{1}{2}\left(\pm\mathbf{t}(x_1) + \frac{1}{\pi i}\fint_{\Gamma_1}\frac{\mathbf{t}(\xi)}{\xi - x_1}\,\mathrm{d}\xi\right), \quad x_1 \in \Gamma_1 \tag{34}$$

and

$$\mathbf{h}(z) = \frac{1}{2\pi i}\int_{\Gamma_1}\frac{\mathbf{t}(\xi)}{\xi - z}\,\mathrm{d}\xi, \quad z \in \mathbb{C}\setminus\Gamma_1, \tag{35}$$

where $\fint$ is the Cauchy principal integral. Because $\mathbf{h}^{\pm}(x_1)$ are given in terms of the unknown $\mathbf{t}(x_1)$ in (34), we need one more equation, which we obtain from (29). Stroh [7], invoking the positive-definiteness of the stiffness tensor, showed that the matrices $\mathbf{A}$ and $\mathbf{B}$ are non-singular if $\Lambda_1 \neq \Lambda_2$; in particular $\mathbf{B}^{-1}$ exists. Taking the derivative of (29) with respect to x_1, then using (31) and $\overline{\mathbf{B}^{-1}} = (\bar{\mathbf{B}})^{-1}$, we obtain

$$\mathbf{A}\mathbf{B}^{-1}\mathbf{h}^{+}(x_1) - \overline{\mathbf{A}\mathbf{B}^{-1}}\mathbf{h}^{-}(x_1) = \mathbf{v}'(x_1), \quad x_1 \in \Gamma_1, \tag{36}$$

where $\mathbf{v}'(x_1) = \begin{pmatrix} dv_1/dx_1 \\ dv_2/dx_1 \end{pmatrix}$. Eliminating $\mathbf{h}^{-}(x_1)$ from (33), (36) and defining $\mathbf{M} := i\mathbf{A}\mathbf{B}^{-1}$, it follows that

$$(\mathbf{M} + \overline{\mathbf{M}})\mathbf{h}^{+}(x_1) = \overline{\mathbf{M}}\mathbf{t}(x_1) + i\mathbf{v}'(x_1), \quad x_1 \in \Gamma_1. \tag{37}$$

Employing (34) in (37) then provides

$$\frac{\mathbf{M} + \overline{\mathbf{M}}}{2\pi i}\fint_{-L}^{L}\frac{\mathbf{t}(\xi)}{\xi - x_1}\mathrm{d}\xi + \frac{\mathbf{M} - \overline{\mathbf{M}}}{2}\mathbf{t}(x_1) = i\mathbf{v}'(x_1). \tag{38}$$

The matrix $\mathbf{M}$ plays an important role in the study of anisotropic materials. It was first introduced by Ingebrigtsen and Tonning in [11]. Its inverse $\mathbf{M}^{-1}$ is called the *impedance tensor*. It provides a convenient relationship $\mathbf{B} = i\mathbf{M}^{-1}\mathbf{A}$ between the matrices $\mathbf{A}$ and $\mathbf{B}$, which are directly related to the displacement field at a point and traction on a plane passing though that point, as may be seen, for example, in (29) and (30).

For a parabolic indenter with profile $x_2 = -x_1^2/(2R)$, we obtain $dv_2/dx_1 = -x_1/R$. We expand the second component of the vector equation (38) to find

$$\frac{M_{22} + \overline{M}_{22}}{2\pi i}\fint_{-L}^{L}\frac{t_2(\xi)}{\xi - x_1}\mathrm{d}\xi + \frac{M_{22} - \overline{M}_{22}}{2}t_2(x_1) = -i\frac{x_1}{R}. \tag{39}$$

It can be shown that both $\mathbf{M}$ and $\mathbf{M}^{-1}$ are positive-definite Hermitian matrices (see [9], Chap. 6), so that $M_{22} = \overline{M}_{22} > 0$. Therefore, from (39), we obtain

$$\frac{M_{22}}{\pi i}\fint_{-L}^{L}\frac{t_2(\xi)}{\xi - x_1}\mathrm{d}\xi = -i\frac{x_1}{R}, \tag{40}$$

which is a singular integral equation with a Cauchy kernel (see [10]). We may solve (40) to obtain the expression (see [3], Chap. 10) for the traction $t_2(x_1) = \sigma_{22}(x_1, 0) = -p(x_1)$ in the contact region as

$$p(x_1) = \frac{1}{R\,M_{22}}\sqrt{L^2 - x_1^2} \quad \text{on } \Gamma_1. \tag{41}$$

Having obtained $t_2(x_1)$, we note that $v_1(x_1)$ can be easily found using the first component of (38) and the condition $v_1(0) = 0$, which follows, without loss of generality, from the mirror symmetry of the configuration about the x_2-axis.

To find $\sigma_{\text{VM}}(x_1, x_2)$ from (8), we first solve for σ_{11}, σ_{12} and σ_{22} using the RH problem formulated in (33). We write (33) in its component form to obtain

$$h_1^+(x_1) - h_1^-(x_1) = 0 \quad \text{and} \quad h_2^+(x_1) - h_2^-(x_1) = t_2(x_1) = -\frac{1}{R\,M_{22}}\sqrt{L^2 - x_1^2}, \quad x_1 \in \Gamma_1. \tag{42}$$

We solve the scalar RH problems (42), using (35), to obtain

$$h_1(z) = 0, \quad z \in \mathbb{C} \quad \text{and} \quad h_2(z) = -\frac{1}{2\pi i\, R\, M_{22}}\int_{-L}^{L} \frac{\sqrt{L^2 - \xi^2}}{\xi - z}\,d\xi, \quad z \in \mathbb{C} \setminus \Gamma_1. \tag{43}$$

Using (31) and (43), we now obtain $\begin{pmatrix} \dfrac{df_1(z)}{dz} \\ \dfrac{df_2(z)}{dz} \end{pmatrix} = \mathbf{B^{-1}h}(z) = \begin{pmatrix} \hat{B}_{12} \\ \hat{B}_{22} \end{pmatrix} h_2(z)$ in S^+, where $\hat{B}_{ij}$ are the components of $\mathbf{B^{-1}}$. Utilizing relations (28), we then find stress fields at a general point in the homogeneous, anisotropic, linear-elastic half-space as

$$\begin{aligned} \sigma_{21}(x_1, x_2) &= 2\text{Re}[B_{11}\hat{B}_{12}h_2(z_1) + B_{12}\hat{B}_{22}h_2(z_2)], \\ \sigma_{22}(x_1, x_2) &= 2\text{Re}[B_{21}\hat{B}_{12}h_2(z_1) + B_{22}\hat{B}_{22}h_2(z_2)], \\ \text{and} \qquad \sigma_{11}(x_1, x_2) &= 2\text{Re}[B_{11}\Lambda_1\hat{B}_{12}h_2(z_1) + B_{12}\Lambda_2\hat{B}_{22}h_2(z_2)]. \end{aligned} \tag{44}$$

Now, using (3) and (4) in the plane strain condition (6), we find that

$$\sigma_{33}(x_1, x_2) = \begin{pmatrix} a_{3311} & a_{3322} & a_{3312} \end{pmatrix} \begin{bmatrix} a_{1111} & a_{1122} & a_{1112} \\ a_{1122} & a_{2222} & a_{2212} \\ a_{1112} & a_{2212} & a_{1212} \end{bmatrix}^{-1} \begin{pmatrix} \sigma_{11} \\ \sigma_{22} \\ \sigma_{12} \end{pmatrix}, \tag{45}$$

which, along with (44) and (8), immediately provides $\sigma_{\text{VM}}(\mathbf{x})$.

When $\mathbf{S_2}^{-1}\mathbf{S_1}$ is not diagonalizable, which includes the case of an isotropic material, an extension of the method above to find $\mathbf{M}$ is given in Appendix A. We now return to the plane strain indentation of layered media. For a finely-layered medium, we use results from homogenization and obtain an anisotropic homogenized material. On the anisotropic half-space the indentation problem may be solved using results from this section.

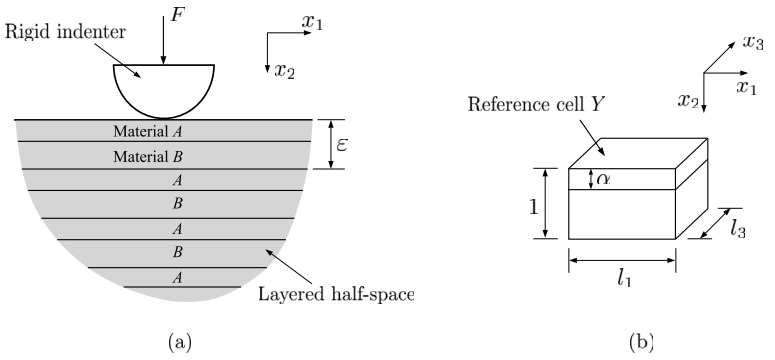

Fig. 2 (**a**) Indentation by a cylindrical indenter of layered half-space with materials A and B stacked as shown. The configuration at any cross-section at x_3 is as shown. (**b**) The reference cell Y; see the main text for details.

4 Indentation on a Layered Medium

4.1 Formulation of the Boundary Value Problem

In a layered medium, in general, two or more different materials are stacked on top of each other in layers that may be repeated in any manner. In this work, we consider layered media in which two different isotropic materials are stacked one after the other in an infinite periodic arrangement, as illustrated in Fig. 2a. We identify material of the topmost layer as 'material A' and the next one as 'material B'. The top two layers with collective thickness ε form a unit, which is then repeated. Thus, the degree of heterogeneity of such layered media may be characterized by a single parameter ε. Let the volume fraction of material A be α, so that the volume fraction of material B is $1-\alpha$. Then, in any unit of ε thickness, material A has thickness $\alpha\,\varepsilon$, and material B's thickness is $(1-\alpha)\,\varepsilon$, so that the thickness ratio is $\alpha/(1-\alpha)$, which is independent of ε.

We introduce the periodic framework for the layered media by defining a *reference cell* $Y := (0, l_1) \times (0, 1) \times (0, l_3)$ for some $l_1 > 0$ and $l_3 > 0$; see Fig. 2b. We define cell $\varepsilon Y := (0, l_1) \times (0, \varepsilon) \times (0, l_3)$. Let the components of the stiffness tensor be functions defined as $a_{ijkh} : Y \to \mathbb{R}$ for $i, j, k, h = 1, 2, 3$. For a layered medium, let $a^{\varepsilon}_{ijkh} : \varepsilon Y \to \mathbb{R}$ for $i, j, k, h = 1, 2, 3$. Set $a^{\varepsilon}_{ijkh}(\mathbf{x}) = a^{\varepsilon}_{ijkh}(x_1, x_2, x_3) = a^{\varepsilon}_{ijkh}(x_2) = a_{ijkh}(x_2/\varepsilon)$. We then extend a^{ε}_{ijkh} periodically to the entire domain Ω to make $a^{\varepsilon}_{ijkh} : \Omega \to \mathbb{R}$ for $i, j, k, h = 1, 2, 3$.

With the above definitions, (1) may then be rewritten as

$$\begin{cases} \dfrac{\partial}{\partial x_j}\left(a^{\varepsilon}_{ijkh}\dfrac{\partial u^{\varepsilon}_k}{\partial x_h}\right) = 0 \quad \text{in } \Omega, \quad i = 1, 2, 3, \\ \dfrac{\partial \mathbf{u}^{\varepsilon}}{\partial x_i} \cdot \mathbf{e_2} = \dfrac{\partial v_2}{\partial x_i}, \quad a^{\varepsilon}_{ijkh}\dfrac{\partial u^{\varepsilon}_k}{\partial x_h} n_j = 0 \quad \text{on } \Gamma_1, \quad i = 1, 3, \\ a^{\varepsilon}_{ijkh}\dfrac{\partial u^{\varepsilon}_k}{\partial x_h} n_j = 0 \quad \text{on } \Gamma_2, \quad i = 1, 2, 3, \end{cases} \tag{46}$$

where $\mathbf{u}^{\varepsilon}(\mathbf{x}) = (u^{\varepsilon}_1(\mathbf{x}), u^{\varepsilon}_2(\mathbf{x}), u^{\varepsilon}_3(\mathbf{x})) : \Omega \to \mathbb{R}^3$ denotes the unknown three-dimensional displacement field in the layered medium.

Accurate FE analysis for finely-layered media, i.e. layered media with very small ε is computationally expensive, as the mesh size becomes correspondingly small. However, for a finely-layered medium, we can proceed by homogenizing the medium. From the theory of periodic homogenization [12, 13], we are led to a consideration of the following boundary value problem:

$$\begin{cases} \dfrac{\partial}{\partial x_j}\left(a^0_{ijkh}\dfrac{\partial u^0_k}{\partial x_h}\right)=0 \quad \text{in } \Omega, \quad i=1,2,3, \\ \dfrac{\partial \mathbf{u}^0}{\partial x_i}\cdot\mathbf{e_2}=\dfrac{\partial v_2}{\partial x_i}, \quad a^0_{ijkh}\dfrac{\partial u^0_k}{\partial x_h}n_j=0 \quad \text{on } \Gamma_1, \quad i=1,3, \\ a^0_{ijkh}\dfrac{\partial u^0_k}{\partial x_h}n_j=0 \quad \text{on } \Gamma_2, \quad i=1,2,3, \end{cases} \tag{47}$$

which is similar to (46), except that the components of the effective stiffness tensor a^0_{ijkh} are now the constant functions representing the homogenized material, and $\mathbf{u}^0(\mathbf{x}) = (u^0_1(\mathbf{x}), u^0_2(\mathbf{x}), u^0_3(\mathbf{x})) : \Omega \to \mathbb{R}^3$ denotes the three-dimensional displacement field of the homogenized material. We now proceed to find the components a^0_{ijkh}.

4.2 Components of the Effective Stiffness Tensor

The components of the stiffness tensor a^0_{ijkh} in (47) are given by [12]

$$a^0_{ijkh}=\frac{1}{|Y|}\int_Y a_{ijkh}(x)\,dx-\frac{1}{|Y|}\int_Y a_{ijlm}(x)\frac{\partial \chi^{kh}_l}{\partial x_m}\,dx, \tag{48}$$

where $|Y| = l_1 l_3$ is the Lebesgue measure of Y and $\boldsymbol{\chi}^{lm} = (\chi^{lm}_k)_{1\le k\le 3} : Y \to \mathbb{R}^3$ for $l, m = 1, 2, 3$ is a vector-valued function, which is a solution of the following periodic auxiliary problem:

$$\begin{cases} \dfrac{\partial}{\partial x_j}\left(a_{ijkh}\dfrac{\partial \chi^{lm}_k}{\partial x_h}\right)=\dfrac{\partial a_{ijlm}}{\partial x_j} \quad \text{in } Y, \\ \chi^{lm}_k \text{ is } Y\text{-periodic}, \\ \mathcal{M}_Y(\chi^{lm}_k)=0, \end{cases} \tag{49}$$

for $1 \le i, j, k, h, l, m \le 3$ and

$$\mathcal{M}_Y(\chi^{lm}_k)=\frac{1}{|Y|}\int_\Omega \chi^{lm}_k(y)dy$$

is the mean value of χ^{lm}_k over Y. Like a_{ijkh}, the tensor a^0_{ijkh} is positive-definite and obeys the same symmetry relations [12].

We first solve the auxiliary problem (49) to obtain $\boldsymbol{\chi}^{lm}$ (see Appendix B). Using (48), we then compute the components of the stiffness tensor of the homogenized material. We obtain (see Appendix C):

$$\begin{aligned} a^0_{1111} &= (\lambda_A+2\mu_A)\alpha+(\lambda_B+2\mu_B)(1-\alpha) \\ &\quad -\frac{(\lambda_A-\lambda_B)^2}{(\lambda_A+2\mu_A)(1-\alpha)+(\lambda_B+2\mu_B)\alpha}\alpha(1-\alpha), \end{aligned}$$

$$
\begin{aligned}
a^0_{1122} &= \lambda_A\alpha + \lambda_B(1-\alpha) - \frac{(\lambda_A-\lambda_B)\left[(\lambda_A+2\mu_A)-(\lambda_B+2\mu_B)\right]}{(\lambda_A+2\mu_A)(1-\alpha)+(\lambda_B+2\mu_B)\alpha}\alpha(1-\alpha),\\
a^0_{1133} &= \lambda_A\alpha + \lambda_B(1-\alpha) - \frac{(\lambda_A-\lambda_B)^2}{(\lambda_A+2\mu_A)(1-\alpha)+(\lambda_B+2\mu_B)\alpha}\alpha(1-\alpha),\\
a^0_{2222} &= (\lambda_A+2\mu_A)\alpha + (\lambda_B+2\mu_B)(1-\alpha)\\
&\quad - \frac{\left[(\lambda_A+2\mu_A)-(\lambda_B+2\mu_B)\right]^2}{(\lambda_A+2\mu_A)(1-\alpha)+(\lambda_B+2\mu_B)\alpha}\alpha(1-\alpha),\\
a^0_{2323} &= \mu_A\alpha + \mu_B(1-\alpha) - \frac{(\mu_A-\mu_B)^2}{\mu_A(1-\alpha)+\mu_B\alpha}\alpha(1-\alpha),\\
a^0_{1313} &= \mu_A\alpha + \mu_B(1-\alpha),\\
a^0_{2233} &= a^0_{1122}, \quad a^0_{3333} = a^0_{1111}, \quad \text{and} \quad a^0_{1212} = a^0_{2323}.
\end{aligned}
\tag{50}
$$

Many of the other coefficients may be computed using symmetry relations of a^0_{ijkh}, e.g. $a^0_{2211} = a^0_{1122}$, or $a^0_{3113} = a^0_{1313}$. All other coefficients are zero. As a rule, all coefficients having any two indices equal and the other two unequal are zero, while coefficients with two pairs of equal indices are non-zero, e.g. $a^0_{1321} = 0$ and $a^0_{1223} = 0$, but $a^0_{1331} \neq 0$.

Because $a^0_{1111} \neq a^0_{2222}$, the homogenized material is clearly *anisotropic*. We note from (50) that only five different a^0_{ijkh} are required to fully characterize the homogenized material, with $a^0_{1313} = (a^0_{1111} - a^0_{1133})/2$. The resulting homogenized material is thus *transversely isotropic* with x_2-axis being its axis of symmetry. From the formulae above we see that the coefficients a^0_{ijkh} satisfy (7). The indentation problem for the homogenized material is therefore a special case of the plane strain indentation problem considered in Sect. 3, and we use results from there to find $p(x_1)$ and $\sigma_{\mathrm{VM}}(\mathbf{x})$ in the next section.

4.3 Contact Pressure and the von Mises Stress in the Homogenized Material

Although subsequent calculations can be done for a layered medium with arbitrary $\alpha \leq 1$, for brevity we consider here a special case with $\alpha = 1/2$, i.e. the layers of both materials are of the same thickness. When $\varepsilon \to 0$, the contact pressure $p(x_1)$ and the von Mises stress $\sigma_{\mathrm{VM}}(\mathbf{x})$ in the homogenized material may be solved by employing results of Sect. 3; this we now present. We first compute matrices $\mathbf{Q}$, $\mathbf{R}$ and $\mathbf{W}$ utilizing the definitions (19) with a^0_{ijkh} calculated in (50), and then diagonalize $\mathbf{S_2}^{-1}\mathbf{S_1}$ to find

$$
\Lambda_1 = i\sqrt{\left(\frac{\lambda_A+\mu_A+\mu_B}{\lambda_A+2\mu_A}\right)\frac{\mu_A}{\mu_B}} \quad \text{and} \quad \Lambda_2 = i\sqrt{\left(\frac{\lambda_B+\mu_A+\mu_B}{\lambda_B+2\mu_B}\right)\frac{\mu_B}{\mu_A}}. \tag{51}
$$

We assume that $\Lambda_1 \neq \Lambda_2$. Therefore, $\mathbf{B}$ is nonsingular, as discussed in Sect. 3. We solve for $\mathbf{A}$, $\mathbf{B}$, and $\mathbf{M} = i\mathbf{A}\mathbf{B}^{-1}$ to obtain

$$
\mathbf{A} = -\frac{1}{2\mu_A\mu_B}\begin{bmatrix} \mu_A & \mu_B \\ \Lambda_1\mu_B & \Lambda_2\mu_A \end{bmatrix}, \quad \mathbf{B} = \begin{bmatrix} -\Lambda_1 & -\Lambda_2 \\ 1 & 1 \end{bmatrix},
$$

$$
\mathbf{M} = \frac{-i}{2(\Lambda_2-\Lambda_1)}\begin{bmatrix} \dfrac{1}{\mu_B}-\dfrac{1}{\mu_A} & \dfrac{\Lambda_2}{\mu_B}-\dfrac{\Lambda_1}{\mu_A} \\ \dfrac{\Lambda_1}{\mu_A}-\dfrac{\Lambda_2}{\mu_B} & \Lambda_1\Lambda_2\left(\dfrac{1}{\mu_B}-\dfrac{1}{\mu_A}\right) \end{bmatrix},
$$

which immediately provides the contact pressure $p(x_1)$ with (41).

The Poisson's ratio for most engineering materials does not vary much. With the assumption that the two isotropic materials A and B constituting the layered medium have the same value ν of Poisson's ratio, we rewrite M_{22} and $p(x_1)$ in terms of the Young's moduli E_A and E_B and ν as

$$M_{22} = \frac{1}{2}\frac{1+\nu}{\sqrt{1-\nu}}\frac{E_A - E_B}{\sqrt{E_A E_B}}\left\{E_A\sqrt{\frac{E_B}{(1-2\nu)E_A + E_B}} - E_B\sqrt{\frac{E_A}{(1-2\nu)E_B + E_A}}\right\}^{-1} \tag{52}$$

and

$$p(x_1) = \frac{2}{R}\frac{\sqrt{1-\nu}}{1+\nu}\frac{\sqrt{E_A E_B}}{E_A - E_B}\left\{E_A\sqrt{\frac{E_B}{(1-2\nu)E_A + E_B}} - E_B\sqrt{\frac{E_A}{(1-2\nu)E_B + E_A}}\right\} \times \sqrt{L^2 - x_1^2}. \tag{53}$$

We note from (53) that as $E_B \to E_A$, i.e. as the layered medium tends to a homogeneous, isotropic medium,

$$p(x_1) \to \frac{1}{R}\frac{E_A}{2(1-\nu^2)}\sqrt{L^2 - x_1^2}, \tag{54}$$

which is precisely the contact pressure profile (11) for a homogeneous, isotropic half-space.

Next, using (44), we obtain

$$\begin{aligned}
\sigma_{21}(x_1, x_2) &= 2\Lambda_1\Lambda_2 \mathrm{Re}\left\{\frac{1}{\Lambda_1 - \Lambda_2}h_2(z_1) - \frac{1}{\Lambda_1 - \Lambda_2}h_2(z_2)\right\}, \\
\sigma_{22}(x_1, x_2) &= 2\mathrm{Re}\left\{\frac{\Lambda_2}{\Lambda_2 - \Lambda_1}h_2(z_1) - \frac{\Lambda_1}{\Lambda_2 - \Lambda_1}h_2(z_2)\right\}, \\
\text{and} \quad \sigma_{11}(x_1, x_2) &= 2\Lambda_1\Lambda_2 \mathrm{Re}\left\{\frac{\Lambda_1}{\Lambda_1 - \Lambda_2}h_2(z_1) - \frac{\Lambda_2}{\Lambda_1 - \Lambda_2}h_2(z_2)\right\},
\end{aligned} \tag{55}$$

where $h_2(z)$ is given by (43). Because $a^0_{1112} = a^0_{2212} = a^0_{1233} = 0$ for the homogenized material, as discussed in Sect. 4.2, we obtain from (45) that

$$\sigma_{33}(x_1, x_2) = \begin{pmatrix} a^0_{1133} & a^0_{2233} \end{pmatrix}\begin{bmatrix} a^0_{1111} & a^0_{1122} \\ a^0_{1122} & a^0_{2222} \end{bmatrix}^{-1}\begin{pmatrix} \sigma_{11}(x_1, x_2) \\ \sigma_{22}(x_1, x_2) \end{pmatrix}, \tag{56}$$

which then immediately provides σ_{VM} from (8).

Note that as the layers become thicker, i.e. as $\varepsilon \to \infty$, the case $0 < \alpha < 1$ represents, in physical terms, the indentation of a half-space consisting of only material A, which is homogeneous and isotropic. At the same time, $\alpha = 1$ implies the absence of material B, i.e. $\alpha = 1$ represents the indentation of a half-space consisting of material A for an arbitrary ε. Similarly, for arbitrary ε, $\alpha = 0$ signifies the indentation of a half-space consisting only of material B, which is also homogeneous and isotropic. All of these cases correspond to the indentation of a homogeneous, isotropic half-space.

5 Numerical Results and Discussion

As mentioned in Sect. 1, homogenization works best in the bulk. However, in an indentation problem we are primarily interested in fields defined on the surface, such as the contact pressure $p(x_1)$. To analyze the merits of homogenization near the boundary, we employ finite element (FE) simulations to investigate indentation on layered media ($\varepsilon > 0$) and find $p(x_1)$; closed-form solutions are not known for a layered medium when $\varepsilon > 0$. We then show, with the help of an appropriately defined error measure, that the pressure profile for the layered medium ($\varepsilon > 0$) converges to that of the homogenized material as $\varepsilon \to 0$. The upper bound of this error is also discussed, and is shown to depend only upon the ratio of the Young's moduli of the two materials in the layered media and their Poisson's ratio ν, which is taken to be the same for both.

We also find the von Mises stress σ_{VM} in the layered media ($\varepsilon > 0$). As we will demonstrate, σ_{VM} is discontinuous across the layers for a layered medium with $\varepsilon > 0$. However, for the corresponding homogenized material σ_{VM} is a continuous function. Because the maximum of σ_{VM} is important to predict the onset of yielding, it is of interest to investigate how well the maximum of the numerically obtained discontinuous σ_{VM} for a layered medium with $\varepsilon > 0$ is estimated by the σ_{VM} found from the corresponding homogenized material.

Indentation of a layered medium with $\varepsilon > 0$ is solved numerically using the commercial FE analysis software ABAQUS [14]. Because of the assumed plane strain deformation, we consider a two-dimensional model in the x_1-x_2 plane utilizing plane strain elements. As we will compare the results from FE simulations done on a *finite* rectangular block of the layered medium to analytical solutions for a *half-space* comprised of the corresponding homogenized material, we take the block of layered medium in the FE computations 'large enough' to reduce the effect of finiteness of the block. We take the finite block of size $(-M_1, M_1) \times (0, M_2)$ with $M_1 > L > 0$ and $M_2 > 0$. Invoking the symmetry of the configuration about the x_2-axis then allows us to simulate only the part $(0, M_1) \times (0, M_2)$. The appropriate size of the block $M_1 = M_2 = 100$ mm is obtained through the FE analysis for an indentation of a block of isotropic material, which acts as a benchmark. In the subsequent analysis, the force F and the corresponding pressure $p(x_1)$ are related by

$$F = \int_0^L p(x_1)\mathrm{d}x_1, \tag{57}$$

where L is the contact length. Thus, the total force on the indenter would be $2F$. We use a circular indenter with radius R, such that $R \gg L$.

We recall that we set $\alpha = 1/2$, i.e. layers of both the materials are of equal thickness, and take their Poisson's ratio to have the same value ν. We define $\gamma := E_A/E_B$, where E_A and E_B are the Young's moduli of the materials A and B, respectively.

The FE solution for the contact pressure distribution for a layered medium of finite size, and characterized by ε, is denoted by $p^{\varepsilon}_{\mathrm{num}}$, which we consider to be a good estimate of the true p^{ε}. We define the relative error

$$\mathcal{E}^{\varepsilon}_{\mathrm{rel}} := \frac{||p^{\varepsilon}_{\mathrm{num}} - p_{\mathrm{hom}}||_{L^2(0,\infty)}}{||p_{\mathrm{hom}}||_{L^2(0,\infty)}}, \tag{58}$$

where $||\cdot||_{L^2(0,\infty)} = \left(\int_0^\infty |\cdot|^2\,\mathrm{d}x_1\right)^{1/2}$ is the L^2-norm and p_{hom} is the contact pressure during indentation of the half-space made up of the homogenized material, the analytical expression

of which is given by (53). In the present case, i.e. the homogenized medium for $\alpha = 1/2$ and $\nu_A = \nu_B = \nu$, with the help of (52), we obtain

$$M_{22} = \frac{1}{E_A} \frac{(1+\nu)(\gamma-1)}{\sqrt{2(1-\nu)}} \left\{ \sqrt{\frac{\gamma}{(1-2\nu)\gamma+1}} - \frac{1}{\sqrt{1-2\nu+\gamma}} \right\}^{-1}. \tag{59}$$

Using (11), (41) and (57), the contact length during the indentation of the homogenized half-space and of an isotropic half-space, here denoted by L_{hom} and L_{iso}, respectively, can be expressed as

$$L_{\text{hom}} = 2\sqrt{\frac{FR}{\pi} M_{22}} \quad \text{and} \quad L_{\text{iso}} = 2\sqrt{\frac{FR}{\pi} \frac{2(1-\nu^2)}{E}}. \tag{60}$$

Again, utilizing (11), (41), and (57) we obtain

$$||p_{\text{hom}}||^2_{L^2(0,\infty)} = \frac{16}{3\pi^{3/2}} \frac{F^{3/2}}{\sqrt{RM_{22}}} \quad \text{and} \quad ||p_{\text{iso}}||^2_{L^2(0,\infty)} = \frac{8\sqrt{2}}{3\pi^{3/2}} \frac{F^{3/2}}{\sqrt{R(1-\nu^2)/E}}, \tag{61}$$

where p_{iso} is the contact pressure during indentation of an isotropic half-space. We observe from (58) that the non-dimensional $\mathcal{E}^{\varepsilon}_{\text{rel}}$ depends upon five dimensional variables: the force F on the indenter, Young's moduli E_A and E_B, the parameter ε which characterizes the heterogeneity, and the radius R of the indenter. Using the Buckingham Π theorem [15], we find three independent non-dimensional parameters relevant to the problem: $F/(E_A R)$, ε/R and γ $(= E_A/E_B)$, so that we must have a functional relationship of the form

$$\mathcal{E}^{\varepsilon}_{\text{rel}} = f\left(\frac{F}{E_A R}, \frac{\varepsilon}{R}, \gamma \right). \tag{62}$$

As we will see below, as $F/(E_A R) \to \infty$, or $\varepsilon/R \to 0$, or $\gamma \to 1$, we will have $\mathcal{E}^{\varepsilon}_{\text{rel}} \to 0$. However, as $F/(E_A R) \to 0$, or $\varepsilon/R \to \infty$, $\mathcal{E}^{\varepsilon}_{\text{rel}} \to \mathcal{E}_{\text{rel,sup}}$, an *upper* bound that depends only upon γ and ν. We estimate the upper bound $\mathcal{E}_{\text{rel,sup}}$ by noting that the elastic response of the layered medium tends to that of the half-space made of material A when $F/(E_A R) \to 0$ or as $\varepsilon/R \to \infty$. This happens because the effect of layers from the second onwards becomes increasingly less at small $F/(E_A R)$ or large ε/R. We explain this by observing that, if we keep ε/R fixed, $F/(E_A R)$ can be reduced either by lowering F, or by augmenting either E_A or R. If $F \to 0$, all layers after the top layer become increasingly less significant, as the deformation due to the indentation does not propagate deep enough. Similarly, as E_A is raised, the top layer becomes stiffer and starts to support a greater amount of load without transmitting it to the lower layers. On the other hand, if R increases, so does ε in order to keep ε/R fixed. A growth in ε indicates thicker layers, which, in turn, means that the top layer now shares an even more significant fraction of the load F.

Now, if we fix $F/(E_A R)$, ε/R may be augmented either by increasing ε or by reducing R. The effect of the former was described above. However, as R is reduced, F/E_A also has to be correspondingly lowered to keep $F/(E_A R)$ fixed. But F/E_A may be lowered either by decreasing F or by raising E_A, the effects of which were explained in the preceding paragraph. Those arguments indicate that the role of the materials below the top layer lessens progressively, and $p^{\varepsilon}_{\text{num}} \to p_A$, which is the contact pressure when the elastic half-space is made entirely of material A when $F/(E_A R) \to 0$ or $\varepsilon/R \to \infty$. This suggests that $\mathcal{E}_{\text{rel,sup}}$ may be obtained by replacing $p^{\varepsilon}_{\text{num}}$ in (58) by p_A to obtain

$$\mathcal{E}_{\text{rel,sup}} = \frac{||p_A - p_{\text{hom}}||_{L^2(0,\infty)}}{||p_{\text{hom}}||_{L^2(0,\infty)}},$$

or
$$\left(\mathcal{E}_{\text{rel,sup}}\right)^2 = \frac{1}{\displaystyle\int_0^\infty p_{\text{hom}}^2(x_1)\mathrm{d}x_1}\left\{\int_0^\infty p_{\text{hom}}^2(x_1)\mathrm{d}x_1 + \int_0^\infty p_A^2(x_1)\mathrm{d}x_1 - 2\int_0^\infty p_A(x_1)\,p_{\text{hom}}(x_1)\mathrm{d}x_1\right\}. \tag{63}$$

Setting $E = E_A$ in (60) and employing (61), we find

$$\left(\int_0^\infty p_A^2(x_1)\mathrm{d}x_1\right) / \left(\int_0^\infty p_{\text{hom}}^2(x_1)\mathrm{d}x_1\right) = \sqrt{\frac{M_{22}E_A}{2(1-\nu^2)}},$$

so that the first two terms in (63) are now known. We now compute the last term in (63). It is convenient to consider the cases $\gamma > 1$, i.e. $E_A > E_B$, $\gamma < 1$ and $\gamma = 1$ separately. First, we note that using (60) provides

$$\frac{L_A}{L_{\text{hom}}} = \sqrt{\frac{2(1-\nu^2)}{M_{22}E_A}} \quad \text{and} \quad \frac{L_B}{L_{\text{hom}}} = \sqrt{\frac{2(1-\nu^2)}{M_{22}E_B}} = \frac{L_A}{L_{\text{hom}}}\sqrt{\gamma}. \tag{64}$$

Considering first $\gamma > 1$, we utilize in (59) and (64) the fact that $\nu < 1/2$ for an isotropic, linear-elastic material (see [16], Chap. 6), so that $L_A < L_{\text{hom}} < L_B$. Because $p_A(x_1) = 0$ outside the contact region, i.e. for $x_1 > L_A$, we find from (11) and (41) that

$$\int_0^\infty p_A(x_1)\,p_{\text{hom}}(x_1)\mathrm{d}x_1 = \frac{1}{2R^2}\frac{E_A}{M_{22}(1-\nu^2)}\int_0^{L_A}\sqrt{L_A^2 - x_1^2}\sqrt{L_{\text{hom}}^2 - x_1^2}\mathrm{d}x_1. \tag{65}$$

The integral in (65) may be expressed in terms of complete elliptic integrals of the first and second kinds denoted by $K(m)$ and $E(m)$, respectively, in terms of the modulus $m = L_A^2/L_{\text{hom}}^2$ (see [17], Chap. 17). Because $m < 1$, we can express K and E as convergent power series to obtain

$$\begin{aligned}
&\int_0^{L_A}\sqrt{L_A^2 - x_1^2}\sqrt{L_{\text{hom}}^2 - x_1^2}\mathrm{d}x_1 \\
&= \frac{1}{3}L_{\text{hom}}\left\{\left(L_A^2 - L_{\text{hom}}^2\right)K\left(\frac{L_A^2}{L_{\text{hom}}^2}\right) + \left(L_A^2 + L_{\text{hom}}^2\right)E\left(\frac{L_A^2}{L_{\text{hom}}^2}\right)\right\} \\
&= \frac{\pi}{4}L_{\text{hom}}L_A^2\left\{1 - \frac{1}{8}\left(\frac{L_A}{L_{\text{hom}}}\right)^2 - \frac{1}{64}\left(\frac{L_A}{L_{\text{hom}}}\right)^4 - \frac{5}{1024}\left(\frac{L_A}{L_{\text{hom}}}\right)^6 + \mathcal{O}\left(\frac{L_A}{L_{\text{hom}}}\right)^7\right\}.
\end{aligned} \tag{66}$$

Combining (61), (63), and (64)–(66), we finally find

$$\mathcal{E}_{\text{rel,sup}} = \left[1 + \sqrt{\frac{M_{22}E_A}{2(1-\nu^2)}} - \frac{3\pi}{4}\left\{1 - \frac{1}{8}\left(\frac{2(1-\nu^2)}{M_{22}E_A}\right) - \frac{1}{64}\left(\frac{2(1-\nu^2)}{M_{22}E_A}\right)^2 + \mathcal{O}\left(\frac{2(1-\nu^2)}{M_{22}E_A}\right)^3\right\}\right]^{1/2}. \tag{67}$$

As is clear from (59), $M_{22}E_A$, and hence $\mathcal{E}_{\text{rel,sup}}$, depends only upon γ and ν. We note again from (59) that $M_{22}E_A \to \infty$ as $\gamma \to \infty$. Therefore, from (67), $\mathcal{E}_{\text{rel,sup}} \to \infty$ as $\gamma \to \infty$.

On the other hand, when $\gamma < 1$, i.e. $E_A < E_B$, we again use (59) and (64) to find that $L_A > L_{\text{hom}} > L_B$. Because $p_{\text{hom}}(x_1) = 0$ for $x_1 > L_{\text{hom}}$, we utilize (11) and (41) again to obtain

$$\int_0^\infty p_A(x_1)\, p_{\text{hom}}(x_1)\mathrm{d}x_1 = \frac{1}{2R^2}\frac{E_A}{M_{22}(1-\nu^2)}\int_0^{L_{\text{hom}}} \sqrt{L_A^2 - x_1^2}\sqrt{L_{\text{hom}}^2 - x_1^2}\mathrm{d}x_1. \tag{68}$$

As before, the integral in (68) may be written in terms of $K\left(L_{\text{hom}}^2/L_A^2\right)$ and $E\left(L_{\text{hom}}^2/L_A^2\right)$, and also as a convergent power series because $L_{\text{hom}} < L_A$. This is then combined with (61), (63) and (64) to find

$$\mathcal{E}_{\text{rel,sup}} = \left[1 + \sqrt{\frac{M_{22}E_A}{2(1-\nu^2)}} - \frac{3\pi}{4}\sqrt{\frac{M_{22}E_A}{2(1-\nu^2)}}\left\{1 - \frac{1}{8}\left(\frac{M_{22}E_A}{2(1-\nu^2)}\right) - \frac{1}{64}\left(\frac{M_{22}E_A}{2(1-\nu^2)}\right)^2 + \mathcal{O}\left(\frac{M_{22}E_A}{2(1-\nu^2)}\right)^3\right\}\right]^{1/2}, \tag{69}$$

which, using (59), again shows that $\mathcal{E}_{\text{rel,sup}}$ depends only upon γ and ν.

We note from (59) that

$$\lim_{\gamma\to 0}\frac{M_{22}E_A}{2(1-\nu^2)} = \sqrt{\frac{1-2\nu}{8(1-\nu)^3}} =: \kappa. \tag{70}$$

Therefore, using (70) in (69), we obtain

$$\lim_{\gamma\to 0}\mathcal{E}_{\text{rel,sup}} = \left[1 + \sqrt{\kappa} - \frac{3\pi}{4}\sqrt{\kappa}\left\{1 - \frac{1}{8}\kappa - \frac{1}{64}\kappa^2 + \mathcal{O}\left(\kappa^3\right)\right\}\right]^{1/2}, \tag{71}$$

where $\kappa = \kappa(\nu)$ is defined in (70).

Turning to $\gamma = 1$, i.e. $E_A = E_B$, and employing (59), we observe that $M_{22}E_A \to 2(1-\nu^2)$ as $\gamma \to 1$. Also, from (64), as L_{hom} always lies in between L_A and L_B, we must have $L_A = L_{\text{hom}} = L_B$ at $\gamma = 1$. This is expected because, for a given ν, $\gamma = 1$ implies that the two materials of the layered medium are the same, so that $p_A = p_{\text{hom}}$. Subsequently, for $\gamma = 1$, (63) implies that $\mathcal{E}_{\text{rel,sup}} = 0$.

We now perform FE simulations and analyze $\mathcal{E}_{\text{rel}}^{\varepsilon}$ by varying the three non-dimensional parameters $F/(E_A R)$, ε/R and γ in turn. Figure 3a shows the variation of $\mathcal{E}_{\text{rel}}^{\varepsilon}$ with ε/R on log-log scale for parameter sets $\{F/(E_A R) = 0.0001, \gamma = 2\}$ and $\{F/(E_A R) = 0.0002, \gamma = 2\}$. We see that at larger values of ε/R, the presence of material B is felt less, giving rise to a high value of $\mathcal{E}_{\text{rel}}^{\varepsilon}$ in both cases. As ε/R is lessened, either by decreasing ε or increasing R, the two materials A and B begin to 'mix' more, thereby reducing $\mathcal{E}_{\text{rel}}^{\varepsilon}$. At a given value of ε/R, $\mathcal{E}_{\text{rel}}^{\varepsilon}$ diminishes as we augment $F/(E_A R)$, which may be accomplished either by raising F or by lowering E_A and/or R. As we raise F, more layers under the indenter begin to get affected by the impressed load, and $\mathcal{E}_{\text{rel}}^{\varepsilon}$ declines. We achieve the same effect if we lower E_A which, for a fixed $\gamma = E_A/E_B$, implies the presence of layers with softer materials. Thus, more layers under the indenter are affected, so that $\mathcal{E}_{\text{rel}}^{\varepsilon}$ shrinks. Lowering R, while keeping ε/R constant requires decreasing ε as well, which indicates thinner layers, i.e. more mixing of the two materials, again resulting in a smaller $\mathcal{E}_{\text{rel}}^{\varepsilon}$. We note that as ε/R grows, both curves

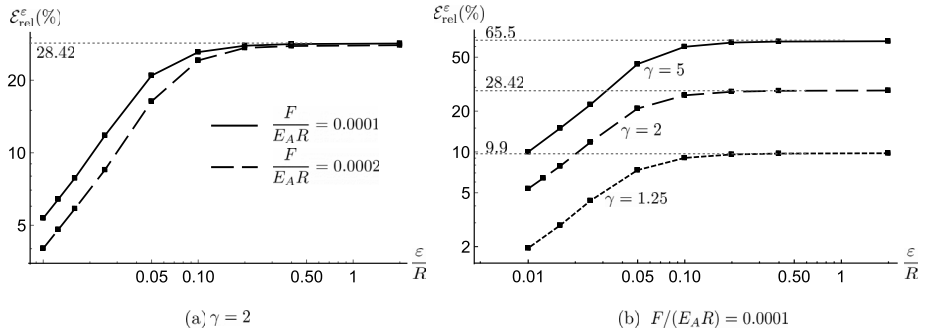

Fig. 3 Log-log plot of variations of $\mathcal{E}^{\varepsilon}_{\text{rel}}$ with ε/R when (**a**) $\gamma = 2$ is held fixed but $F/(E_A R)$ varied, and (**b**) γ varied, while $F/(E_A R) = 0.0001$ is held fixed. The square dots represent the points where $\mathcal{E}^{\varepsilon}_{\text{rel}}$ was found numerically, which were then joined by straight lines.

tend to the same $\mathcal{E}_{\text{rel,sup}}$ because γ is kept unchanged. Using (67), we find $\mathcal{E}_{\text{rel,sup}} = 28.42\%$ for $\gamma = 2$, which matches with the numerical results; see Fig. 3a.

In Fig. 3b we show the log-log plot of $\mathcal{E}^{\varepsilon}_{\text{rel}}$'s variation with ε/R for a fixed value of $F/(E_A R) = 0.0001$, but for three different values of $\gamma = 1.25, 2$, and 5. At higher values of ε/R, we have the same situation as described above, i.e. at higher ε/R layers become thicker and the presence of material B is felt less, thereby raising $\mathcal{E}^{\varepsilon}_{\text{rel}}$ in all cases. As we reduce ε/R, the materials get better mixed, so that $\mathcal{E}^{\varepsilon}_{\text{rel}}$ lowers. However, we note that, for a given ε/R, $\mathcal{E}^{\varepsilon}_{\text{rel}}$ varies greatly with γ. As we increase γ beyond 1, the elastic response of the corresponding homogenized material becomes progressively more different from that of either of its constituents due to the increased contrast in the elastic response of the two layers. Thus, for a given ε/R, $\mathcal{E}^{\varepsilon}_{\text{rel}}$ is largest when γ is furthest from 1. We also note that for $\gamma = 1$, both materials have the same elastic response and the layered medium is now homogeneous and isotropic, so that $\mathcal{E}^{\varepsilon}_{\text{rel}} = 0$ for all ε/R. We observe that as ε/R grows, all three curves tend to different $\mathcal{E}_{\text{rel,sup}}$ as per (67), because γ is different in each case. Using (67), we find $\mathcal{E}_{\text{rel,sup}} = 65.5\%$, 28.42%, and 9.9% for $\gamma = 5, 2$ and 1.25, respectively, which are in excellent match with the numerical results in Fig. 3b.

Next, we present in Fig. 4 the log-log plot of the variation of $\mathcal{E}^{\varepsilon}_{\text{rel}}$ with $F/(E_A R)$. In Fig. 4a, we set $\gamma = 2$, and investigate $\varepsilon/R = 0.025$ and $\varepsilon/R = 0.0125$. As we augment $F/(E_A R)$, $\mathcal{E}^{\varepsilon}_{\text{rel}}$ reduces due to the deeper influence of the applied load, thereby involving more layers in load sharing. For a given $F/(E_A R)$, as we raise ε/R, the layers thicken, so that materials mix less and $\mathcal{E}^{\varepsilon}_{\text{rel}}$ increases.

In Fig. 4b, we set $\varepsilon/R = 0.025$ and consider $\gamma = 0.5$ and $\gamma = 2$. We note that for high values of $F/(E_A R)$, $\mathcal{E}^{\varepsilon}_{\text{rel}}$ is lower when $\gamma = 2$ than when $\gamma = 0.5$. For a fixed $E_A = E^0_A$, $\gamma = 2$ results in layers with materials having Young's moduli E^0_A and $E_B = 0.5E^0_A$, whereas $\gamma = 0.5$ provides E^0_A and $E_B = 2E^0_A$. Therefore, $\gamma = 0.5$ yields layers with stiffer materials than when $\gamma = 2$. For a large given value of $F/(E_A R)$, fewer layers participate in load sharing in the half-space with stiffer layers, leading to a larger value of $\mathcal{E}^{\varepsilon}_{\text{rel}}$. However, as explained previously, if $F/(E_A R)$ gets smaller, the top layer supports the most load and other layers become progressively less important. Using (67) and (69), we find $\mathcal{E}_{\text{rel,sup}} = 28.42\%$ for $\gamma = 2$, but $\mathcal{E}_{\text{rel,sup}} = 21.18\%$ for $\gamma = 0.5$. Because of this reversal in the magnitudes of $\mathcal{E}^{\varepsilon}_{\text{rel}}$ for $\gamma = 2$ and $\gamma = 0.5$, the two curves in Fig. 4b cross each other as $F/(E_A R)$ is increased.

Finally, we report the change of $\mathcal{E}^{\varepsilon}_{\text{rel}}$ with γ in Fig. 5. In Fig. 5a, we fix $\varepsilon/R = 0.025$ and probe the effect of $F/(E_A R) = 0.0001$ and $F/(E_A R) = 0.0004$ on $\mathcal{E}^{\varepsilon}_{\text{rel}}$. Evidently, $\mathcal{E}^{\varepsilon}_{\text{rel}}$ increases as we move away from $\gamma = 1$, because then the two materials get progressively more

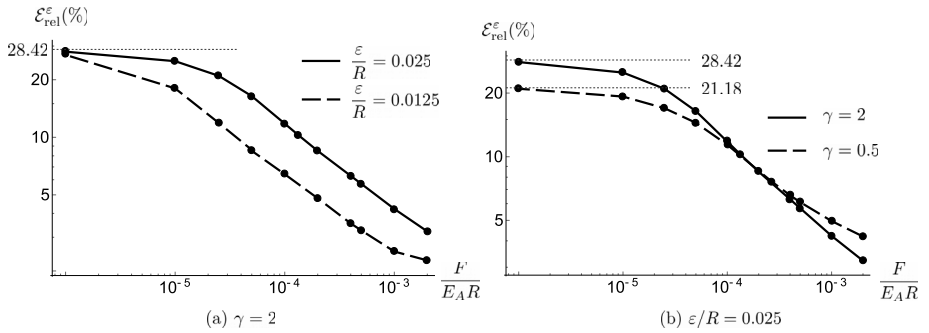

Fig. 4 Log-log plot of variations of $\mathcal{E}^{\varepsilon}_{\text{rel}}$ with $F/(E_A R)$ when (**a**) $\gamma = 2$ is held fixed but ε/R varied, and (**b**) γ is varied, while $\varepsilon/R = 0.025$ is held fixed. We denote the points where $\mathcal{E}^{\varepsilon}_{\text{rel}}$ was found numerically by circular dots, which were then joined by straight lines.

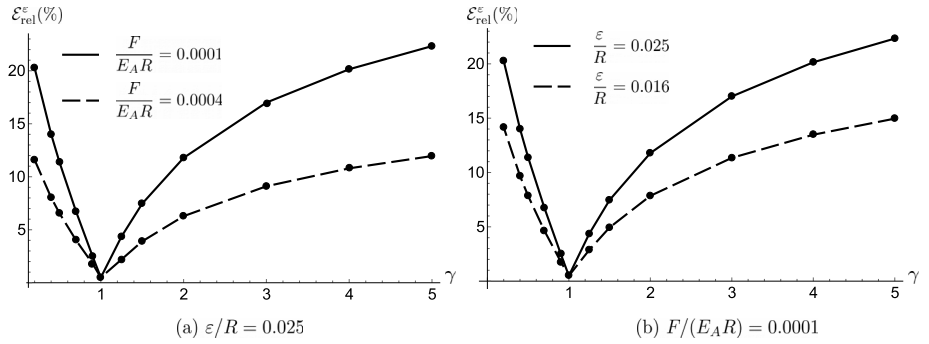

Fig. 5 Variation of $\mathcal{E}^{\varepsilon}_{\text{rel}}$ with γ when (**a**) $\varepsilon/R = 0.025$ is held fixed but $F/(E_A R)$ varied, and (**b**) ε/R varied, while $F/(E_A R) = 0.0001$ is held fixed. As described in the main text, $\mathcal{E}^{\varepsilon}_{\text{rel}} = 0$ at $\gamma = 1$. The circular dots, except at $\gamma = 1$, represent the points where $\mathcal{E}^{\varepsilon}_{\text{rel}}$ was found numerically, which were then joined by straight lines.

different elastically, so that homogenization results in a homogenized material with elastic properties substantially different from those of either of the two constituent materials. Also, as before, for a given value of γ, $\mathcal{E}^{\varepsilon}_{\text{rel}}$ reduces as we raise $F/(E_A R)$ for reasons discussed previously. Similarly, in Fig. 5b, we set $F/(E_A R) = 0.0001$ and take $\varepsilon/R = 0.016$ and $\varepsilon/R = 0.025$. At a given value of γ, $\mathcal{E}^{\varepsilon}_{\text{rel}}$ reduces as we lower ε/R, as the layers get thinner, yielding a better mix of the two materials.

Figure 6 explores the error landscape in the space of any two of the three non-dimensional parameters – γ, ε/R, and $F/(E_A R)$ – while the third is kept fixed. The shaded region in Fig. 6 depicts the parameter range which limits $\mathcal{E}^{\varepsilon}_{\text{rel}}$ to within 5%. In Fig. 6a, $F/(E_A R)$ is kept fixed at 0.0001, while γ and ε/R are varied. We observe that as we move away from $\gamma = 1$, ε/R needs to reduce in order to keep $\mathcal{E}^{\varepsilon}_{\text{rel}} \leq 5\%$. A large $|\gamma - 1|$ indicates greater dissimilarity between the Young's moduli of the layers' materials, so that we need to correspondingly reduce ε/R to increase mixing and keep $\mathcal{E}^{\varepsilon}_{\text{rel}} \leq 5\%$. Near $\gamma = 1$, we find two critical γ's – $\gamma_1 < 1$ and $\gamma_2 > 1$ – that depend upon $F/(E_A R)$, such that the error $\mathcal{E}^{\varepsilon}_{\text{rel}}$ is independent of ε/R when $\gamma \in (\gamma_1, \gamma_2)$. This happens because, for $\gamma \in (\gamma_1, \gamma_2)$, the layered materials and the resulting homogenized material have very similar elastic properties which nullifies the effect of ε/R on $\mathcal{E}^{\varepsilon}_{\text{rel}}$. This may also be explained by observing that for

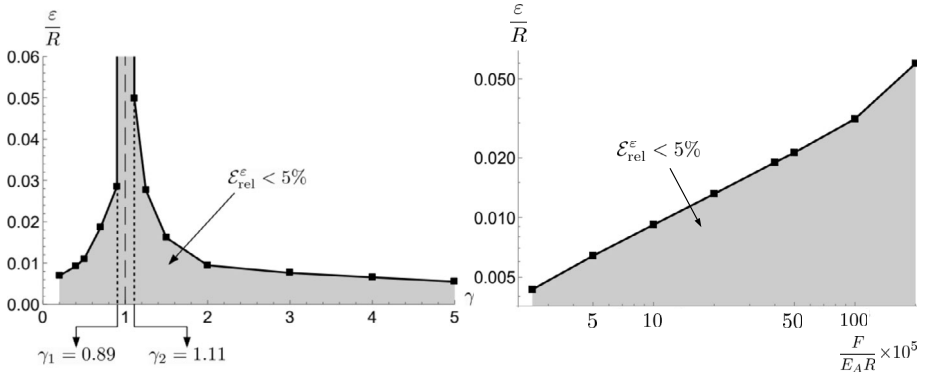

(a) Contour Plot: $F/E_A R = 0.0001$ (b) Log-log contour Plot: $\gamma = 2$

Fig. 6 Regions in parameter space that limit the error $\mathcal{E}^{\varepsilon}_{\text{rel}}$ to within the prescribed limit of 5%. The shaded region corresponds to $\mathcal{E}^{\varepsilon}_{\text{rel}} < 5\%$. In (**a**) $F/(E_A R)$ is held constant, whereas in (**b**) γ is fixed. The dotted vertical lines at γ_1 and γ_2 in (**a**) define the region where $\mathcal{E}^{\varepsilon}_{\text{rel}}$ is independent of ε/R. We denote the points where $\mathcal{E}^{\varepsilon}_{\text{rel}}$ was numerically found by the square dots, which were then joined by straight lines.

given $F/(E_A R)$ and ε/R, $\mathcal{E}_{\text{rel,sup}}$ tends to zero continuously as $\gamma \to 1$. Therefore, there will exist $\gamma_1 < 1$ and $\gamma_2 > 1$, such that $\mathcal{E}_{\text{rel,sup}} \leq 5\%$ for all $\gamma_1 < \gamma < \gamma_2$. Using (69) and (67), respectively, we find that $\gamma_1 = 0.89$ and $\gamma_2 = 1.11$, which match numerical results; see Fig. 6a.

Figure 6b represents the error landscape in log-log scale after setting $\gamma = 2$. Clearly, at larger $F/(E_A R)$, ε/R can take up higher values while still maintaining $\mathcal{E}^{\varepsilon}_{\text{rel}} \leq 5\%$, because large $F/(E_A R)$ leads to more layers getting involved in load sharing, as described previously. As we increase ε/R, the first layer progressively supports a greater percentage of the load, and the effect of material B becomes increasingly less significant. Thus, at a given $F/(E_A R)$, ε/R beyond a critical value leads to an error greater than 5%.

Figure 7 is similar to the Fig. 6, except that the shaded region depicts the permissible values of the two non-dimensional parameters which restrict $\mathcal{E}^{\varepsilon}_{\text{rel}} \leq 10\%$. Here also, we find two critical γ's, $\gamma_1 < 1$ and $\gamma_2 > 1$, such that the error $\mathcal{E}^{\varepsilon}_{\text{rel}}$ is independent of ε/R when $\gamma \in (\gamma_1, \gamma_2)$. Utilizing (69) and (67), respectively, we find that $\gamma_1 = 0.77$ and $\gamma_2 = 1.25$, which again match the numerical results shown in Fig. 7a.

We now compare our predictions with those obtained from the rule of mixtures, which is a simple mechanics of materials approach to find the effective elastic coefficients for layered material. We find four effective elastic coefficients from the rule of mixtures, denoted by E_{11}, E_{22}, ν_{12} and μ_{12}, as follows (see [18]):

$$E_{11} = \alpha E_A + (1-\alpha) E_B, \quad E_{22} = \left(\frac{\alpha}{E_A} + \frac{1-\alpha}{E_B} \right)^{-1},$$

$$\nu_{12} = \alpha \nu_A + (1-\alpha) \nu_B, \quad \text{and} \quad \mu_{12} = \left(\frac{\alpha}{\mu_A} + \frac{1-\alpha}{\mu_B} \right)^{-1}.$$

Then, employing the following relationship between stress and strain components,

$$\begin{pmatrix} \epsilon_{11} \\ \epsilon_{22} \\ \epsilon_{12} \end{pmatrix} = \begin{bmatrix} 1/E_{11} & -\nu_{12}/E_{11} & 0 \\ -\nu_{12}/E_{11} & 1/E_{22} & 0 \\ 0 & 0 & 1/\mu_{12} \end{bmatrix} \begin{pmatrix} \sigma_{11} \\ \sigma_{22} \\ \sigma_{12} \end{pmatrix} \tag{72}$$

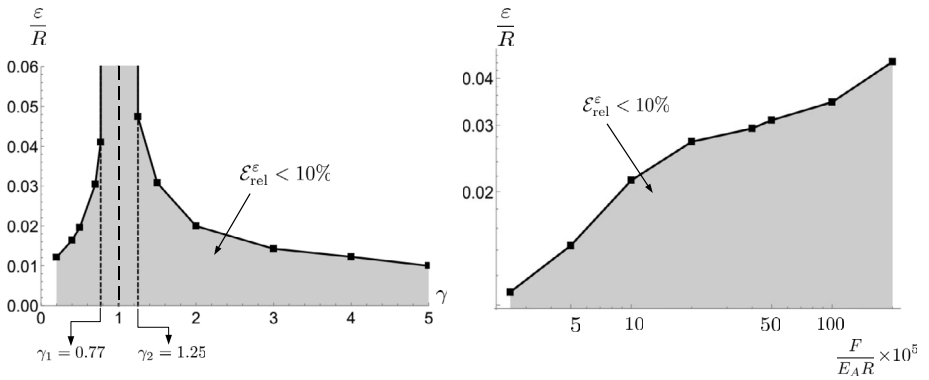

(a) Contour Plot: $F/E_A R = 0.0001$ (b) Log-log contour Plot: $\gamma = 2$

Fig. 7 Regions in parameter space that limit the error $\mathcal{E}^{\varepsilon}_{\text{rel}}$ to within 10%. In (**a**) $F/(E_A R)$ is held constant, whereas in (**b**) γ is fixed. The dotted vertical lines at γ_1 and γ_2 in (**a**) define the region where $\mathcal{E}^{\varepsilon}_{\text{rel}}$ is independent of ε/R. The square dots represent the points where $\mathcal{E}^{\varepsilon}_{\text{rel}}$ was numerically found, which were then joined by straight lines.

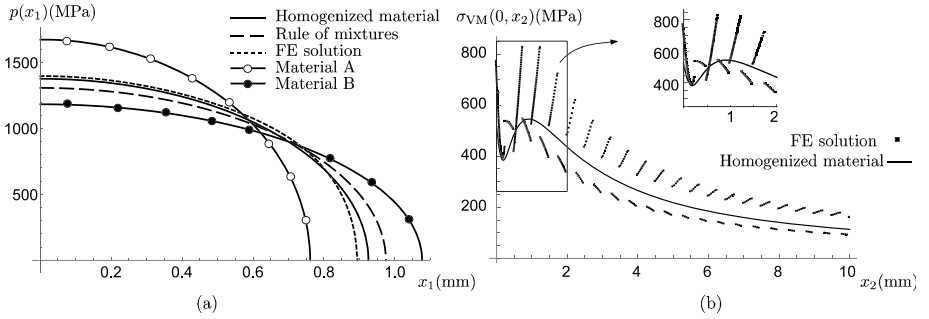

Fig. 8 (**a**) Comparison between the contact pressure $p(x_1)$ in the effective materials obtained with rule of mixtures and with homogenization. The Young's moduli are $E_A = 200$ GPa and $E_B = 100$ GPa. The FE solution for the contact pressure with $\varepsilon/R = 0.01$ is also shown, along with contact pressure that would be obtained if the half-space was made of only material A or material B. (**b**) The variation of $\sigma_{\text{VM}}(0, x_2)$ with depth x_2 at $x_1 = 0$ for $E_A = 200$ GPa, $E_B = 40$ GPa and $\varepsilon/R = 0.01$. Both the FE solution for the layered medium and the analytical solution obtained for the corresponding homogenized material are shown. Dots represent the nodes of the mesh in the numerical solution. In both (**a**) and (**b**), we keep $F = 1000$ N/mm, $\nu = 0.3$ and $R = 50$ mm fixed.

yields, after inversion of the square matrix and using (3), the components a_{ijkh} of the stiffness tensor of the effective material as estimated by the rule of mixtures. Figure 8a depicts the difference in the contact pressure obtained by using the rule of mixtures and through homogenization (Sect. 4.3). We find that the rule of mixtures produces an effective medium with lower stiffness than the one found through homogenization. Also, the FE solution is closer to the homogenized solution than with the one found using rule of mixtures, demonstrating that homogenization provides a better approximation to the true solution.

As mentioned in Sect. 2, the von Mises stress σ_{VM} is an important quantity that is often utilized to predict the onset of yielding. We consider a layered medium with $\nu = 0.3$, $E_A = 200$ GPa, and $E_B = 40$ GPa, so that $\gamma = 5$. We take $F = 1000$ N/mm, $\varepsilon/R = 0.01$ and the

indenter's radius $R = 50$ mm. We observe numerically that $\sigma_{\rm VM}$ takes its maximum on the x_2-axis, i.e. at $x_1 = 0$. Figure 8b compares $\sigma_{\rm VM}$ along the x_2-axis obtained by employing the analytical results for the homogenized material with that found from FE computations for a material with $\varepsilon/R = 0.01$. As detailed in Sect. 4.3, to find $\sigma_{\rm VM}$ on the x_2-axis for the homogenized material, we first find stress components by substituting $z_i = \Lambda_i x_2$ for $i = 1, 2$ in (55) to obtain

$$\begin{aligned}
\sigma_{21}(0, x_2) &= 0, \\
\sigma_{22}(0, x_2) &= \frac{1}{R\,M_{22}} \left\{ -\frac{\Lambda_2}{\Lambda_2 - \Lambda_1} \left(i\,\Lambda_1 x_2 + \sqrt{L^2 - \Lambda_1^2 x_2^2} \right) \right. \\
&\quad \left. + \frac{\Lambda_1}{\Lambda_2 - \Lambda_1} \left(i\,\Lambda_2 x_2 + \sqrt{L^2 - \Lambda_2^2 x_2^2} \right) \right\}, \\
\sigma_{11}(0, x_2) &= \frac{\Lambda_1 \Lambda_2}{R\,M_{22}} \left\{ \frac{\Lambda_1}{\Lambda_1 - \Lambda_2} \left(i\,\Lambda_1 x_2 + \sqrt{L^2 - \Lambda_1^2 x_2^2} \right) \right. \\
&\quad \left. - \frac{\Lambda_2}{\Lambda_1 - \Lambda_2} \left(i\,\Lambda_2 x_2 + \sqrt{L^2 - \Lambda_2^2 x_2^2} \right) \right\},
\end{aligned} \tag{73}$$

where we have utilized the purely imaginary nature of Λ_i, as is clear from (51) and the relation $h_2(\Lambda_i x_2) = -1/(RM_{22})(i\,\Lambda_i x_2 + \sqrt{L^2 - \Lambda_i^2 x_2^2})$ evaluated using contour integration and the residue theorem from complex analysis. We may obtain $\sigma_{33}(0, x_2)$ using (56), which when employed with (73) in (8) immediately provides $\sigma_{\rm VM}(0, x_2)$. We clearly observe that $\sigma_{\rm VM}(0, x_2)$ in the homogenized material is a continuous function of x_2. In the layered medium, however, a discontinuity in $\sigma_{\rm VM}$ across layers results from the discontinuity of σ_{11}, and hence of σ_{33}. Note that both σ_{12} and σ_{22} are continuous across layers because of the physical requirement that traction be continuous at an interface. The homogenized material provides a good approximation of the average behavior of $\sigma_{\rm VM}$. However, near the surface, calculations with the homogenized medium underestimate the maximum value of $\sigma_{\rm VM}$ in the layered medium found from FE computations. It is interesting to note that as ε reduces further, $\sigma_{\rm VM}$ becomes discontinuous at more points but, obviously, $\sigma_{\rm VM}$ remains continuous for the homogenized material.

We now investigate the relationship of the maximum of $\sigma_{\rm VM}$ for the homogenized, anisotropic material with the maximum of $\sigma_{\rm VM}$ found after assuming that the half-space is made of material A or material B that comprise the layered medium. We consider two different layered half-spaces defined by the sets $\{E_A = 200$ GPa, $E_B = 160$ GPa$\}$ and $\{E_A = 200$ GPa, $E_B = 30$ GPa$\}$. We set $F = 1000$ N/mm, $\nu = 0.3$ and $R = 50$ mm for both cases. We have already confirmed numerically that $\sigma_{\rm VM}$ achieves its maximum on the x_2-axis. We then analytically obtain $\sigma_{\rm VM}(0, x_2)$ for the homogenized material as discussed in the previous paragraph. To find $\sigma_{\rm VM}(0, x_2)$ for each of the constituent homogeneous, isotropic materials, i.e. materials A and B, we substitute $z = i x_2$ in (13) and (15) and employ (8) to obtain

$$\begin{aligned}
&\sigma_{\rm VM}(0, x_2) \\
&= \frac{4\mu}{R(\chi + 1)} \left[\frac{\left\{ L^2 + 2x_2 \left(x_2 - \sqrt{x_2^2 + L^2} \right) \right\} \left\{ L^2 (1 - 2\nu)^2 + 4x_2^2 \left(1 - \nu + \nu^2 \right) \right\}}{x_2^2 + L^2} \right]^{1/2}.
\end{aligned}$$

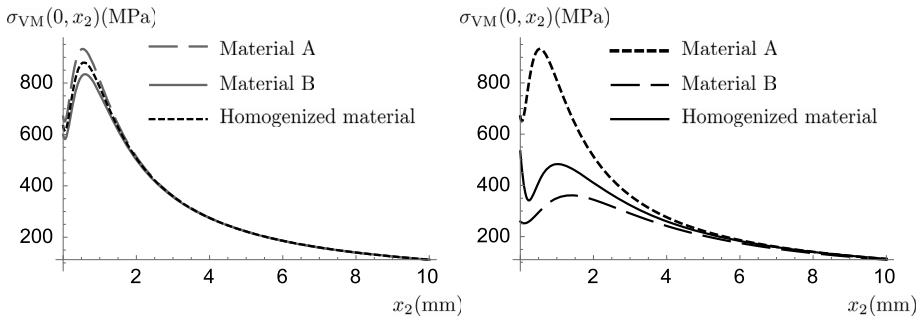

(a) $E_A = 200\text{GPa}, E_B = 160\text{GPa}$ (b) $E_A = 200\text{GPa}, E_B = 30\text{GPa}$

Fig. 9 The variation of $\sigma_{\rm VM}(x_2)$ with x_2 during the indentations of half-spaces made either of material A or B that constitute the layered medium and the corresponding homogenized material. Two different types of layered media are considered. We keep $F = 1000$ N/mm, $\nu = 0.3$ and $R = 50$ mm fixed.

We find that for materials A and B, and for the homogenized material, $\sigma_{\rm VM}$ can achieve its maximum either at $x_2 = 0$, or somewhere below the contact surface, i.e. at $x_2 > 0$. As shown in Fig. 9a, for the layered medium with $E_A = 200$ GPa and $E_B = 160$ GPa, the maximum of the homogenized material is at $x_2 > 0$, whereas Fig. 9b shows that by changing the Young's modulus of material B from 160 GPa to 30 GPa, the maximum in $\sigma_{\rm VM}$ for the homogenized material shifts from $x_2 > 0$ to $x_2 = 0$. However, in Fig. 9b, $\sigma_{\rm VM}$ takes its maximum at $x_2 > 0$ whenever the half-space is made only of material A or B. At the same time, $\sigma_{\rm VM}$ of the homogenized material always remains sandwiched between the $\sigma_{\rm VM}$ corresponding to a half-space comprised only of material A or material B.

We end this section with a remark. The discrepancy between the FE solution $p^{\varepsilon}_{\rm num}$ and the analytical solution $p_{\rm hom}$ for the contact pressure is due to both the non-inclusion of boundary layer corrector and the finite layer thickness ε/R. In the present work, we have not attempted to distinguish between the two sources of the discrepancy. This would require including the boundary layer corrector, which is a complex calculation. Here, the aim of comparing $p^{\varepsilon}_{\rm num}$ and $p_{\rm hom}$ was to gauge the accuracy – and hence the applicability – of the leading-order estimate ($p_{\rm hom}$) obtained using homogenization. To this end, we have demonstrated above that the relative error (in the L_2 norm) between $p^{\varepsilon}_{\rm num}$ and $p_{\rm hom}$ converges to zero as $\varepsilon/R \to 0$. Depending upon the maximum acceptable error, we find the range of layer thicknesses (see e.g. Figs. 6, 7), for which the indentation into layered media can be solved using homogenization, without the added complexity of including the boundary layer corrector. The addition of the latter will increase the range of ε/R, for which the error is within a prescribed bound, by hastening the convergence rate of the results of homogenization to the actual solution when $\varepsilon/R \to 0$.

6 Conclusions

We analyzed plane strain indentation of a periodically layered half-space, which is an example of a heterogeneous medium. We homogenized the half-space when the layer thickness ε is small, which physically represents a finely mixed composite medium, and obtained closed-form expressions for the components of the effective stiffness tensor of the homogenized material. We found that the homogenized material is anisotropic. We separately obtained analytical expressions for the contact pressure for indentation into an anisotropic,

homogeneous half-space, and used that solution to investigate the indentation of the homogenized medium. We demonstrated, by analyzing an appropriately defined error variable, that the contact pressure on the layered medium, found through FE computations, tends to that obtained by homogenization, when we either reduce the layer thickness ε/R, or augment the applied force $F/(E_A R)$, or make $\gamma = E_A/E_B$ tend to 1, demonstrating the merits of homogenization in an indentation problem. It was also shown that the upper bound of this error depends solely upon γ and the Poisson's ratio of the layers' materials. We also observed that this error found through homogenization is lower than the error that we obtain if we utilize the rule of mixtures to replace the layered half-space by a homogeneous medium.

We then obtained analytical expressions for the von Mises stress σ_{VM} – a scalar field often used to predict the onset of yielding – during indentation of isotropic and anisotropic, homogeneous half-spaces and, through FE computations, of the layered medium. We then investigated σ_{VM}'s maximum, which occurs either at the indenter's tip, or below the surface on the vertical axis passing through its tip, and observed that σ_{VM} in the layered medium is discontinuous at the interfaces between the layers. Employing homogenization underestimates the maximum of this σ_{VM}, but does capture the average behavior.

The approach presented here can be utilized for a diverse array of indentation and contact problems of finely mixed heterogeneous media, for which numerics is expensive and complex. As demonstrated here, it is possible to approximate such problems by an analogous one posed for a suitably homogenized medium, wherein numerics are simpler and which may even permit an exact analytical solution, as in our case.

Finally, our approach is amenable to systematic improvements. Indeed, it is well known that the homogenization of a heterogeneous medium provides the leading-order term correctly in the two-scale asymptotic expansion of a given field variable in terms of its heterogeneity. However, the boundary layer corrector, if ignored from the first order onward, leads to sub-optimal convergence of relevant fields, such as the contact pressure, as the degree of heterogeneity tends to zero. We are currently incorporating the influence of the boundary layers at first order to help improve the estimates made through homogenization.

Acknowledgements T. M. acknowledges the support from Indo-French Centre for Applied Mathematics (IFCAM) and DST-MATRICS Project no. MTR/2017/000587.

Appendix A: Evaluation of M for Isotropic Materials

For cases when $\mathbf{S_2}^{-1}\mathbf{S_1}$ is not diagonalizable, which happens only if $\Lambda_1 = \Lambda_2 = \Lambda$, we can still find a nonsingular matrix $\hat{\mathbf{E}}$, such that

$$\hat{\mathbf{E}}^{-1}\mathbf{S_2}^{-1}\mathbf{S_1}\hat{\mathbf{E}} = \begin{bmatrix} \Lambda & 1 & 0 & 0 \\ 0 & \Lambda & 0 & 0 \\ 0 & 0 & \bar{\Lambda} & 1 \\ 0 & 0 & 0 & \bar{\Lambda} \end{bmatrix}, \tag{74}$$

where the square matrix on the right is the Jordan normal form of $\mathbf{S_2}^{-1}\mathbf{S_1}$. We can then extend the definition of $\mathbf{M}$ to such cases by writing $\hat{\mathbf{E}}$ in terms of two 2×2 nonsingular matrices $\mathbf{A}$ and $\mathbf{B}$, as done in (25). We let $\hat{\mathbf{E}} = \left[\begin{smallmatrix} \mathbf{A} & \bar{\mathbf{A}} \\ \mathbf{B} & \bar{\mathbf{B}} \end{smallmatrix}\right]$ and define $\mathbf{M} = i\mathbf{A}\mathbf{B}^{-1}$ as done in Sect. 3.

For an isotropic material with Lamé's parameters λ and μ, we find matrices $\mathbf{Q}$, $\mathbf{R}$ and $\mathbf{W}$ using (10) and (19) to be

$$\mathbf{Q} = \begin{bmatrix} \lambda+2\mu & 0 \\ 0 & \mu \end{bmatrix}, \quad \mathbf{R} = \begin{bmatrix} 0 & \lambda \\ \mu & 0 \end{bmatrix} \quad \text{and} \quad \mathbf{W} = \begin{bmatrix} \mu & 0 \\ 0 & \lambda+2\mu \end{bmatrix}. \tag{75}$$

While diagonalizing $\mathbf{S_2}^{-1}\mathbf{S_1}$ with (75), we find $\Lambda_1 = \Lambda_2 = i$, corresponding to which we obtain only one independent eigenvector. Therefore, the matrix $\mathbf{S_2}^{-1}\mathbf{S_1}$ for an isotropic material, obtained using (75) is not diagonalizable. Hence, we use its Jordan normal form (74) to compute $\hat{\mathbf{E}}$, so that

$$\mathbf{S_2}^{-1}\mathbf{S_1} = \hat{\mathbf{E}} \begin{bmatrix} i & 1 & 0 & 0 \\ 0 & i & 0 & 0 \\ 0 & 0 & -i & 1 \\ 0 & 0 & 0 & -i \end{bmatrix} \hat{\mathbf{E}}^{-1},$$

$$\text{where} \quad \hat{\mathbf{E}} = \begin{bmatrix} -\dfrac{1}{2\mu} & i\dfrac{\lambda+2\mu}{2\mu(\lambda+\mu)} & -\dfrac{1}{2\mu} & -i\dfrac{\lambda+2\mu}{2\mu(\lambda+\mu)} \\ -\dfrac{i}{2\mu} & \dfrac{1}{2(\lambda+\mu)} & \dfrac{i}{2\mu} & \dfrac{1}{2(\lambda+\mu)} \\ -i & -1 & i & -1 \\ 1 & 0 & 1 & 0 \end{bmatrix}. \tag{76}$$

We now easily find $\mathbf{A}$, $\mathbf{B}$ and $\mathbf{M}$, as done in (25) to obtain

$$\mathbf{A} = \begin{bmatrix} -\dfrac{1}{2\mu} & i\dfrac{\lambda+2\mu}{2\mu(\lambda+\mu)} \\ -\dfrac{i}{2\mu} & \dfrac{1}{2(\lambda+\mu)} \end{bmatrix}, \ \mathbf{B} = \begin{bmatrix} -i & -1 \\ 1 & 0 \end{bmatrix}$$

$$\text{and} \quad \mathbf{M} = \frac{1}{2(\lambda+\mu)} \begin{bmatrix} \dfrac{\lambda+2\mu}{\mu} & i \\ -i & \dfrac{\lambda+2\mu}{\mu} \end{bmatrix}. \tag{77}$$

In particular, we obtain from (77) that $M_{22} = (\chi+1)/4\mu$, where we recall that $\chi = (\lambda+3\mu)/(\lambda+\mu)$. Thus, for an isotropic material, (41) reduces to (11), as it should.

We, however, cannot use the matrix $\mathbf{B}$ thus obtained in (44) when $\mathbf{S_2}^{-1}\mathbf{S_1}$ is not diagonalizable, because in such a case the general solutions (24), which crucially depend upon this diagonalization, no longer hold and need modification. Therefore, for indentation of an isotropic material, we require a different approach. We follow the results obtained by Muskhelishvili [19], which we compiled at the end of Sect. 2. Muskhelishvili employed a similar complex variables based approach as given in Sect. 3, but employing the structure of an isotropic material right from the beginning, thereby bypassing the problem of lack of diagonalization of $\mathbf{S_2}^{-1}\mathbf{S_1}$.

Appendix B: Solutions of the Auxiliary Periodic Problem

We solve auxiliary problem (49) for $\boldsymbol{\chi}^{lm}$, which are then used in (48) to find the components of the effective stiffness tensor of the homogenized material. For $l = 1$, $m = 1$ and $i = 1$,

the PDE

$$\frac{\partial}{\partial x_j}\left(a_{ijkh}\frac{\partial \chi_k^{lm}}{\partial x_h}\right)=\frac{\partial a_{ijlm}}{\partial x_j}$$

in (49) transforms to

$$\frac{\partial}{\partial x_1}\left(a_{1111}\frac{\partial \chi_1^{11}}{\partial x_1}+a_{1122}\frac{\partial \chi_2^{11}}{\partial x_2}+a_{1133}\frac{\partial \chi_3^{11}}{\partial x_3}\right)+\frac{\partial}{\partial x_2}\left(a_{1212}\frac{\partial \chi_1^{11}}{\partial x_2}+a_{1221}\frac{\partial \chi_2^{11}}{\partial x_1}\right)$$
$$+\frac{\partial}{\partial x_3}\left(a_{1313}\frac{\partial \chi_1^{11}}{\partial x_3}+a_{1331}\frac{\partial \chi_3^{11}}{\partial x_1}\right)=0.$$

The remaining terms in the above expansion are zero either on account of a_{ijkh}'s being zero for appropriate indices, as is clear from (10), or because $a_{ijkh}(\mathbf{x})=a_{ijkh}(x_2)$, which implies $\frac{\partial a_{ijkh}}{\partial x_m}=0$ for $m=1,3$. Using (10), we obtain

$$\frac{\partial}{\partial x_1}\left\{(\lambda+2\mu)\frac{\partial \chi_1^{11}}{\partial x_1}+\lambda\frac{\partial \chi_2^{11}}{\partial x_2}+\lambda\frac{\partial \chi_3^{11}}{\partial x_3}\right\}+\frac{\partial}{\partial x_2}\left(\mu\frac{\partial \chi_1^{11}}{\partial x_2}+\mu\frac{\partial \chi_2^{11}}{\partial x_1}\right)$$
$$+\frac{\partial}{\partial x_3}\left(\mu\frac{\partial \chi_1^{11}}{\partial x_3}+\mu\frac{\partial \chi_3^{11}}{\partial x_1}\right)=0. \tag{78}$$

Similarly, for $l=1$, $m=1$, $i=2$ and $l=1$, $m=1$, $i=3$, we have

$$\frac{\partial}{\partial x_1}\left(\mu\frac{\partial \chi_1^{11}}{\partial x_2}+\mu\frac{\partial \chi_2^{11}}{\partial x_1}\right)+\frac{\partial}{\partial x_2}\left\{\lambda\frac{\partial \chi_1^{11}}{\partial x_1}+(\lambda+2\mu)\frac{\partial \chi_2^{11}}{\partial x_2}+\lambda\frac{\partial \chi_3^{11}}{\partial x_3}\right\}$$
$$+\frac{\partial}{\partial x_3}\left(\mu\frac{\partial \chi_2^{11}}{\partial x_3}+\mu\frac{\partial \chi_3^{11}}{\partial x_2}\right)=\frac{\partial \lambda}{\partial x_2}, \tag{79}$$

and

$$\frac{\partial}{\partial x_1}\left(\mu\frac{\partial \chi_1^{11}}{\partial x_3}+\mu\frac{\partial \chi_3^{11}}{\partial x_1}\right)+\frac{\partial}{\partial x_2}\left(\mu\frac{\partial \chi_2^{11}}{\partial x_3}+\mu\frac{\partial \chi_3^{11}}{\partial x_2}\right)$$
$$+\frac{\partial}{\partial x_3}\left\{\lambda\frac{\partial \chi_1^{11}}{\partial x_1}+\lambda\frac{\partial \chi_2^{11}}{\partial x_2}+(\lambda+2\mu)\frac{\partial \chi_3^{11}}{\partial x_3}\right\}=0, \tag{80}$$

respectively. We solve (78)–(80) for $\boldsymbol{\chi}^{11}(\mathbf{x}):=(\chi_1^{11},\chi_2^{11},\chi_3^{11})$. To this end, we guess that χ_1^{11}, χ_2^{11} and χ_3^{11} are independent of x_1 and x_3, so that (78), (79) and (80) reduce, respectively, to the following:

$$\frac{\partial}{\partial x_2}\left(\mu\frac{\partial \chi_1^{11}}{\partial x_2}\right)=0,\quad \frac{\partial}{\partial x_2}\left\{(\lambda+2\mu)\frac{\partial \chi_2^{11}}{\partial x_2}\right\}=\frac{\partial \lambda}{\partial x_2}\quad\text{and}\quad \frac{\partial}{\partial x_2}\left(\mu\frac{\partial \chi_3^{11}}{\partial x_2}\right)=0.$$

Solving the above set of equations, we obtain

$$\chi_1^{11} = \chi_3^{11} = 0$$

$$\text{and} \quad \chi_2^{11} = \begin{cases} \dfrac{(\lambda_A - \lambda_B)(1-\alpha)}{(\lambda_A + 2\mu_A)(1-\alpha) + (\lambda_B + 2\mu_B)\alpha} \left(x_2 - \dfrac{\alpha}{2}\right), & 0 < x_2 < \alpha, \\ \dfrac{(\lambda_A - \lambda_B)\alpha}{(\lambda_A + 2\mu_A)(1-\alpha) + (\lambda_B + 2\mu_B)\alpha} \left(\dfrac{\alpha+1}{2} - x_2\right), & \alpha < x_2 < 1. \end{cases} \tag{81}$$

Similarly, with the assumption that $\boldsymbol{\chi}^{lm}(\mathbf{x}) = \boldsymbol{\chi}^{lm}(x_2)$ we solve for other $\boldsymbol{\chi}^{lm}$ as given below:

$$\chi_2^{12} = \chi_3^{12} = 0, \quad \chi_1^{12} = \begin{cases} \dfrac{(\mu_A - \mu_B)(1-\alpha)}{\mu_A(1-\alpha) + \mu_B\alpha} \left(x_2 - \dfrac{\alpha}{2}\right), & 0 < x_2 < \alpha, \\ \dfrac{(\mu_A - \mu_B)\alpha}{\mu_A(1-\alpha) + \mu_B\alpha} \left(\dfrac{\alpha+1}{2} - x_2\right), & \alpha < x_2 < 1, \end{cases} \tag{82}$$

$$\boldsymbol{\chi}^{13} = \mathbf{0}, \quad \boldsymbol{\chi}^{21} = \boldsymbol{\chi}^{12},$$

$$\chi_1^{22} = \chi_3^{22} = 0,$$

$$\chi_2^{22} = \begin{cases} \dfrac{[(\lambda_A + 2\mu_A) - (\lambda_B + 2\mu_B)](1-\alpha)}{(\lambda_A + 2\mu_A)(1-\alpha) + (\lambda_B + 2\mu_B)\alpha} \left(x_2 - \dfrac{\alpha}{2}\right), & 0 < x_2 < \alpha, \\ \dfrac{[(\lambda_A + 2\mu_A) - (\lambda_B + 2\mu_B)]\alpha}{(\lambda_A + 2\mu_A)(1-\alpha) + (\lambda_B + 2\mu_B)\alpha} \left(\dfrac{\alpha+1}{2} - x_2\right), & \alpha < x_2 < 1, \end{cases}$$

$$\chi_1^{23} = \chi_2^{23} = 0, \quad \chi_3^{23} = \chi_1^{12},$$

$$\boldsymbol{\chi}^{31} = \boldsymbol{\chi}^{13} = \mathbf{0}, \quad \boldsymbol{\chi}^{32} = \boldsymbol{\chi}^{23}, \quad \text{and} \quad \boldsymbol{\chi}^{33} = \boldsymbol{\chi}^{11}.$$

We note that $\boldsymbol{\chi}^{lm} = \boldsymbol{\chi}^{ml}$.

Appendix C: Components of the Effective Stiffness Tensor

Using (48), we compute the components of the effective stiffness tensor of the homogenized material. We start with a^0_{1111}:

$$a^0_{1111} = \frac{1}{|Y|}\int_Y a_{1111}(x)\,dx - \frac{1}{|Y|}\int_Y \left(a_{1111}\frac{\partial \chi_1^{11}}{\partial x_1} + a_{1112}\frac{\partial \chi_1^{11}}{\partial x_2} + a_{1113}\frac{\partial \chi_1^{11}}{\partial x_3}\right.$$
$$\left. + a_{1121}\frac{\partial \chi_2^{11}}{\partial x_1} + a_{1122}\frac{\partial \chi_2^{11}}{\partial x_2} + a_{1123}\frac{\partial \chi_2^{11}}{\partial x_3} + a_{1131}\frac{\partial \chi_3^{11}}{\partial x_1} + a_{1132}\frac{\partial \chi_3^{11}}{\partial x_2} + a_{1133}\frac{\partial \chi_3^{11}}{\partial x_3}\right) dx.$$

In the second integrand on the right side above several terms vanish identically because, $a_{1112} = a_{1113} = a_{1121} = a_{1123} = a_{1131} = a_{1132} = 0$ from (10). Also $\dfrac{\partial \chi_1^{11}}{\partial x_1} = \dfrac{\partial \chi_3^{11}}{\partial x_3} = 0$ from (81). Thus, we compute

$$a^0_{1111} = \frac{1}{|Y|}\int_Y a_{1111}(x)\,dx - \frac{1}{|Y|}\int_Y a_{1122}(x)\frac{\partial \chi_2^{11}}{\partial x_2}\,dx$$
$$= \frac{l_1 l_3}{|Y|}\left\{\int_0^\alpha (\lambda_A + 2\mu_A)\,dx_2 + \int_\alpha^1 (\lambda_B + 2\mu_B)\,dx_2\right\}$$

$$
\begin{aligned}
&- \frac{l_1 l_3}{|Y|}\left\{\int_0^{\alpha} \frac{\lambda_A(\lambda_A-\lambda_B)(1-\alpha)}{(\lambda_A+2\mu_A)(1-\alpha)+(\lambda_B+2\mu_B)\alpha}\,dx_2\right.\\
&\left.+\int_{\alpha}^{1} \frac{-\lambda_B(\lambda_A-\lambda_B)\alpha}{(\lambda_A+2\mu_A)(1-\alpha)+(\lambda_B+2\mu_B)\alpha}\,dx_2\right\}\\
&=(\lambda_A+2\mu_A)\alpha+(\lambda_B+2\mu_B)(1-\alpha)\\
&\quad-\frac{(\lambda_A-\lambda_B)^2}{(\lambda_A+2\mu_A)(1-\alpha)+(\lambda_B+2\mu_B)\alpha}\alpha(1-\alpha).
\end{aligned}
$$

Next, we calculate a^0_{1112}:

$$
\begin{aligned}
a^0_{1112} &= \frac{1}{|Y|}\int_Y a_{1112}(x)\,dx - \frac{1}{|Y|}\int_Y \left(a_{1111}\frac{\partial \chi_1^{12}}{\partial x_1}+a_{1112}\frac{\partial \chi_1^{12}}{\partial x_2}+a_{1113}\frac{\partial \chi_1^{12}}{\partial x_3}\right.\\
&\quad\left.+a_{1121}\frac{\partial \chi_2^{12}}{\partial x_1}+a_{1122}\frac{\partial \chi_2^{12}}{\partial x_2}+a_{1123}\frac{\partial \chi_2^{12}}{\partial x_3}+a_{1131}\frac{\partial \chi_3^{12}}{\partial x_1}+a_{1132}\frac{\partial \chi_3^{12}}{\partial x_2}+a_{1133}\frac{\partial \chi_3^{12}}{\partial x_3}\right)dx\\
&= 0
\end{aligned}
$$

utilizing (10), along with $\frac{\partial \chi_1^{12}}{\partial x_1}=0$ and $\chi_2^{12}=\chi_3^{12}=0$ from (82). Similarly, we find the other coefficients that are provided in (50).

References

1. Doerner, M.F., Nix, W.D.: A method for interpreting the data from depth-sensing indentation instruments. J. Mater. Res. **1**(4), 601–609 (1986)
2. Oliver, W.C., Pharr, G.M.: An improved technique for determining hardness and elastic modulus using load and displacement sensing indentation experiments. J. Mater. Res. **7**(6), 1564–1583 (1992)
3. Muskhelishvili, N.I., Radok, J.R.M.: Singular Integral Equations: Boundary Problems of Function Theory and Their Application to Mathematical Physics. Dover, New York (2008)
4. Sneddon, I.N.: Fourier Transforms. Dover, New York (1995)
5. Green, A.E., Zerna, W.: Theoretical Elasticity. Oxford (Clarendon) Press, Oxford (1954)
6. Fan, H., Keer, L.: Two-dimensional contact on an anisotropic elastic half-space. J. Appl. Mech. **61**(2), 250–255 (1994)
7. Stroh, A.: Dislocations and cracks in anisotropic elasticity. Philos. Mag. **3**(30), 625–646 (1958)
8. Chen, W.F., Han, D.J.: Plasticity for Structural Engineers. (2007). J. Ross Publishing
9. Ting, T.C.T.: Anisotropic Elasticity: Theory and Applications. No. 45. (1996). Oxford University Press on Demand
10. Gakhov, F.D.: Boundary Value Problems. Pergamon Press Ltd., Elmsford (1986)
11. Ingebrigtsen, K., Tonning, A.: Elastic surface waves in crystals. Phys. Rev. **184**(3), 942–951 (1969)
12. Cioranescu, D., Donato, P.: An Introduction to Homogenization. Oxford University Press, London (1999)
13. Ganesh, S.S., Vanninathan, M.: Bloch wave homogenization of linear elasticity system. ESAIM Control Optim. Calc. Var. **11**(4), 542–573 (2005)
14. Hibbitt, H., Karlsson, B., Sorensen, P.: Abaqus Analysis User's Manual Version 2016. Dassault Systèmes Simulia Corp., Providence (2016)
15. Bridgman, P.W.: Dimensional Analysis. Yale University Press, New Haven (1922)
16. Sadd, M.H.: Elasticity: Theory, Applications, and Numerics. Academic Press, San Diego (2009)
17. Abramowitz, M., Stegun, I.A.: Handbook of Mathematical Functions with Formulas, Graphs, and Mathematical Tables. Dover, New York (1965)
18. Jones, R.M.: Mechanics of Composite Materials. 2E. Taylor & Francis, Philadelphia (1999)
19. Muskhelishvili, N.I., Radok, J.R.M.: Some Basic Problems of the Mathematical Theory of Elasticity. Springer, Berlin (2013)